

1 **A critical evaluation of decadal solar cycle imprints in the MiKlip**
2 **historical ensemble simulations**

3
4 Tobias Christian Spiegl¹, Ulrike Langematz¹, Holger Pohlmann², Jürgen Kröger²

5 ¹Institute of Meteorology, Freie Universität Berlin, Berlin, Germany

6 ²Max Planck Institute for Meteorology, Hamburg, Germany

7
8 *Correspondence to:* T. C. Spiegl (tobias.spiegl@met.fu-berlin.de)

9

10 **Abstract**

11 Studies concerning solar-terrestrial connections over the last decades claim to have found evidence that the quasi-
12 decadal solar cycle can have an influence on the dynamics in the middle atmosphere in the Northern Hemisphere
13 during winter season. It has been argued that feedbacks between the intensity of the UV part of the solar spectrum and
14 low latitude stratospheric ozone may produce anomalies in meridional temperature gradients which have the potential
15 to alter the zonal-mean flow in mid to high latitudes. Interactions between the zonal wind and planetary waves can
16 lead to a downward propagation of the anomalies, produced in the middle atmosphere, down to the troposphere. More
17 recently, it has been proposed that top-down initiated decadal solar signals might modulate surface climate and
18 synchronize the North Atlantic Oscillation. A realistic representation of the solar cycle in climate models was
19 suggested to significantly enhance decadal prediction skill. These conclusions have been debated controversial since
20 then due to the lack of missing realistic decadal prediction model set ups and more extensive analysis.

21 In this paper we aim for an objective and improved evaluation of possible solar imprints from the middle atmosphere
22 to the surface and with that from head to toe. Thus, we analyze model output from historical ensemble simulations
23 conducted with the state-of-the-art Earth system model MPI-ESM-HR. The target of these simulations was to isolate
24 the most crucial model physics to foster basic research on decadal climate prediction and to develop an operational
25 ensemble decadal prediction system within the MiKlip framework.

26 Based on correlations and multiple linear regression analysis we show that the MPI-ESM-HR simulates a realistic,
27 statistically significant and robust shortwave heating rate and temperature response at the tropical stratopause, in good
28 agreement with existing studies. However, the dynamical response to this initial radiative signal in the NH during the
29 boreal winter season is weak. We find a slight strengthening of the polar vortex in midwinter during solar maximum
30 conditions in the ensemble mean, which is consistent with the so-called “top-down” mechanism. The individual
31 ensemble members, however, show a large spread in the dynamical response with opposite signs in response to the
32 solar cycle, which might be a result of the large overall internal variability compensating rather small solar imprints.

33 We also analyze the possible surface responses to the 11-year solar cycle and review the proposed synchronization
34 between the solar forcing and the North Atlantic Oscillation. We find that the simulated westerly wind anomalies in
35 the lower troposphere as well as the anomalies in the mean sea level pressure are most likely independent from the
36 timing of the solar signal in the middle atmosphere and the alleged top-down influences. The pattern rather reflects

37 the decadal internal variability of the troposphere, mimicking positive and negative phases of the Arctic- and North
38 Atlantic Oscillations throughout the year sporadically, which is then assigned to the solar predictor time series without
39 any physical plausible connection and sound solar contribution.

40 Finally, by applying lead/lag correlations, we find that the proposed synchronization between the solar cycle and the
41 decadal component of the North Atlantic Oscillation might rather be a statistical artefact, affected for example by the
42 internal decadal variability of the ocean, than a plausible physical connection between the UV solar forcing and quasi-
43 decadal variations in the troposphere.

44

45 1. Introduction

46 The discipline of decadal climate prediction is rather young and a rapidly growing field in climate science. By using
47 initialized climate model simulations, the gap between weather forecasting and long-term climate model projections
48 covering the complete 21st century or beyond is bridged (e.g., Pohlmann et al., 2013; Meehl et al., 2014). By the aid
49 of decadal climate predictions, policymakers can be equipped with an improved decision-making basis allowing for a
50 better planning of necessary water resources, agriculture, energy and infrastructure measures for the near-term future
51 (Mehta et al., 2011). The aim of the German joint research project “Mittelfristige Klimaprognose” (MiKlip) was to
52 establish a new decadal prediction system allowing for a more precise midterm climate forecasting. To this effect,
53 potential driving factors shaping the decadal climate from both anthropogenic and natural sources have been evaluated
54 critically based on large ensemble simulations with the Max Planck Institute for Meteorology Earth System Model
55 (MPI-ESM).

56 One factor that potentially influences tropospheric weather and climate is the variability in the middle atmosphere via
57 stratosphere-troposphere coupling processes. The internal variability in the middle atmosphere during the dynamically
58 active winter and spring seasons is strongly controlled by the variability of Rossby waves, which propagate upward
59 from the troposphere to the middle atmosphere where they break and interact with the zonal-mean flow. The changes
60 in the zonal-mean flow, again, can alter the propagation conditions for planetary scale waves initiating a self-consistent
61 feedback called wave-mean flow interaction (e.g. Andrews 1985). As a result, strong disruptions, born in the middle
62 atmosphere, such as sudden stratospheric warmings (SSWs), which are characterized by a breakdown of the polar
63 vortex, have the potential to propagate downward into lower atmospheric layers and interfere with the tropospheric
64 weather regime (e.g., Baldwin and Dunkerton, 2001). A prominent example for this are Northern Hemisphere (NH)
65 cold air outbreaks which have the tendency to be more frequent and severe in seasons with a weak stratospheric polar
66 vortex (e.g. Huang et al., 2021).

67 A source of variability that might influence the dynamics in the middle atmosphere on the decadal timescale via a
68 complex feedback mechanism between radiation, chemistry and wave-mean flow interaction is the 11-year solar cycle.
69 Pioneering work concerning the impact of the solar cycle on middle atmosphere dynamics and possible connections
70 to the troposphere goes back to Kodera and Kuroda (2002). Based on a relatively short period of NCEP reanalysis data
71 (1979 – 1998), the authors observed an increase of the tropical stratopause temperature (TST) (at ~50 km) during the

72 time of the solar maximum. In their conceptual explanation, this temperature increase leads to a strengthening of the
73 meridional temperature gradient and an intensification of the polar night jet (PNJ) in the winter stratosphere. The
74 stronger westerlies create a barrier for upward propagating planetary waves, which in turn are deflected poleward and
75 break at lower altitudes. The resulting divergence in the Eliassen-Palm flux (EPF) allows the positive wind anomaly
76 to move downward and poleward over the winter season. Kodera (2002) argues that the solar induced wind anomalies
77 may advance into the troposphere, where they create a signal in meteorological variables mimicking a positive phase
78 of the North Atlantic Oscillation (NAO). Matthes et al. (2004, 2006) studied the proposed “top-down” mechanism by
79 the aid of idealized simulations with an early 3-dimensional middle atmosphere general circulation model (GCM).
80 Analysing monthly to sub-monthly means, they found that during solar maximum conditions the polar vortex seems
81 to be stronger especially in November and December and linked this to a positive Arctic oscillation (AO)-like pattern
82 which they found in lower altitudes and to some extent at the surface. The observed pattern weakens in January and
83 changes sign from February onwards. In subsequent studies comparable results have been found (e.g., Schmidt et al.,
84 2010; Ineson et al., 2011; Chiodo et al., 2012; Langematz et al., 2013). However, the exact timing of the progression
85 of the signals from the middle atmosphere to the surface depends on the individual study and varies from December
86 to February. These early studies are often quoted as convincing proof for a “top-down” influence of the 11-year solar
87 cycle in both the middle atmosphere and the troposphere. Complementary to this, Gray et al. (2013) found that the
88 strongest NAO-like solar-induced signals in the North Atlantic (i.e. a positive phase of the NAO) actually seem to
89 appear with a time lag of three to four years after the solar maximum in the respective seasonal winter mean (DJF).
90 However, the observed lags could not be reproduced in coupled atmosphere-ocean simulations conducted by the same
91 group. In the model, the postulated response to the solar cycle in the North Atlantic appears almost in phase with the
92 solar forcing (maximum response between lag year zero to one) (Gray et al., 2013). This discrepancy between observed
93 and simulated lag in the response in the North Atlantic NAO was confirmed in subsequent studies (e.g., Scaife et al.,
94 2013; Andrews et al., 2015).

95 With respect to possible solar induced impacts on NH surface variability in the winter season, Thiéblemont et al.
96 (2015) went one step further. Analyzing a simulation incorporating 150 model years, they claim that the solar forcing
97 synchronizes the decadal component of the NAO variability spectrum, a phase relation they cannot find in an
98 experiment without 11-year solar variability. This result has been debated controversially since its publication. Chiodo
99 et al. (2019) found almost identical spectra of the NAO decadal variability in two simulations of 500 model years each,

100 with and without a 11-year solar cycle forcing. Furthermore, they identified NAO patterns in similar time segments in
101 both experiments (forced and unforced). They suspect, therefore, that the alleged surface solar signals in other studies
102 are most likely a result of the internal variability of the NAO itself rather than solar cycle imprints. On the other hand,
103 Drews et al. (2022) most recently argue that the solar cycle near-surface imprints can only shine through during very
104 active solar periods with large amplitudes of the 11-year solar cycle. They also state that during these periods the
105 surface decadal prediction skill would be significantly enhanced if the solar cycle is a vital part of the prediction
106 system. In the context of the most recent literature, it is difficult to understand why Chiodo et al. (2019) and Drews et
107 al. (2022) arrive at a different assessment of the solar signal, even though the same model was used. This might point
108 to the fact, that the complexity of the model is not the most relevant component in shaping potential surface solar
109 signals, but rather the effects of internal variability in individual model runs and (to some degree) the applied analysis.

110 In this publication, we evaluate possible imprints of the 11-year solar cycle in different domains of the atmosphere
111 from the initial solar radiative signal in the tropical upper stratosphere down to the surface in the NH winter season.
112 We analyze the MiKlip historical ensemble simulations conducted with the state-of-the-art Earth system model MPI-
113 ESM-HR, which is the physical basis for the decadal prediction system, which is operational at the “Deutscher
114 Wetterdienst” (DWD) since 2020. The availability of the large amount of output data from the MiKlip historical model
115 ensemble enables us to address the unresolved questions of the solar surface imprint, such as the dependence of the
116 signal on the solar cycle amplitude, on a more robust statistical basis than is possible in single model simulations. In
117 our study, we aim to identify the role of the solar imprints for the decadal variability of the NAO in winter. While the
118 model simulations include both, changes in the total solar irradiance (TSI) and spectral solar irradiance (SSI), potential
119 effects related to solar energetic particles (SEP) and medium energy electrons (MEE) are not explicitly included in the
120 MiKlip experiments. Observations and model studies suggest that changes in the stratospheric composition related to
121 SEP can lead to a radiatively driven modulation of the middle atmosphere dynamics, which can penetrate to lower
122 atmospheric layers down to the troposphere (e.g., Seppälä et al., 2009, 2014; Baumgaertner et al., 2010; Arsenovic et
123 al., 2016). However, since no robust surface impacts have been simulated even for strong solar energetic particle
124 events (SEP) of the recent decades (Jackman et al., 2009), we infer that including these effects may not alter our results
125 significantly.

126 This publication is structured as follows. In Section 2 we describe the MPI-ESM, the setup of the analyzed simulations
127 and the applied methodologies to detect potential solar cycle signals in different atmospheric domains. In Section 3,

128 the initial radiative solar signal in the tropical middle atmosphere is evaluated. Subsequently, we concentrate on the
129 dynamical response to the initial solar signal in the NH winter season. Here we show in Section 4 the ensemble mean
130 response and compare individual ensemble members with opposite solar signatures. In Section 5, we derive solar-
131 induced signals near the surface in our simulations and observations. In Section 6, we check our model results with
132 respect to the proposed synchronization between the solar forcing and the NAO. Finally, we summarize and discuss
133 our results in a broader context (Section 7).

134

135 2. Data and methods

136 2.1 Model description and experimental design

137 The historical simulations analyzed in this publication have been conducted with the Max Planck Institute for
138 Meteorology Earth System Model in high resolution configuration (MPI-ESM1.2-HR; hereafter called MPI-ESM-
139 HR) at the Deutsches Klimarechenzentrum (DKRZ). MPI-ESM-HR includes the atmospheric general circulation
140 model ECHAM (European Centre Hamburg) version 6.3 (ECHAM6.3) with a horizontal/vertical resolution of
141 T127L95 (corresponds to a ~ 100 km * 100 km model grid and 95 levels in the vertical with a model top at 0.01 hPa
142 or ~ 80 km) (Müller et al., 2018). The high vertical resolution allows for an internally generated quasi-biennial
143 oscillation (QBO) in the tropical stratosphere (Pohlmann et al., 2019). Radiative processes are represented using the
144 rapid radiation transfer model for GCMs (RRTM-G) for both the shortwave and longwave part of the electromagnetic
145 spectrum (Iacono et al., 2008). Other diabatic processes, such as vertical mixing by turbulence and moist convection,
146 large-scale convection, and momentum deposition by orographic and unresolved gravity waves are described in more
147 detail in Stevens et al. (2013). Oceanic processes are accounted for in the coupled Max Planck Institute ocean model
148 (MPIOM) with a TP0.4 (0.4° nominal) resolution (Jungclaus et al., 2013). MPI-ESM-HR further incorporates the
149 biogeochemistry module Hamburg Model of the Ocean Carbon Cycle (HAMOCC) (Ilyina et al., 2013; Paulsen et al.,
150 2017) and the land surface model JSBACH (Reick et al., 2013).

151 In this publication, we analyze 10 members of the MPI-ESM-HR historical simulations performed within the German
152 research project MiKlip. The MiKlip historical ensemble simulations include the observed natural and anthropogenic
153 climate drivers, as described in the CMIP5 protocol (Taylor et al., 2013). The individual ensemble members (1 to 10)
154 have been initialized from different model years of a 1850 preindustrial (PI) control simulation and were integrated

155 over the period 1850 to 2005. Since especially the very early years are little reliable in observations and the model has
156 been spun-up with a constant solar forcing, we focus on the period 1880 – 1999. Thus, a total of 1,200 model years
157 have been evaluated. Since the model does not include interactive atmospheric chemistry, ozone concentrations have
158 to be prescribed. In the MiKlip historical simulations, the merged CMIP5 ozone dataset was used, which consists of a
159 combination of SAGE I+II satellite and radiosonde data in the period 1979 to 2005. To derive earlier ozone
160 concentrations back to 1850, the zonal mean stratospheric time series is extended backwards based on the regression
161 fits and proxy time series of equivalent effective stratospheric chlorine (EESC) and solar variability (Cionni et al.,
162 2011). The solar variability forcing includes all observed solar cycles and follows Lean (2000).

163

164 2.1 Data analysis

165 *Detrending, correlations, filtering*

166 To detrend the sunspot number (SSN) (Source: WDC-SILSO, Royal Observatory of Belgium, Brussels -
167 <https://www.sidc.be/silso/infosnmtot>) and shortwave heating rate time series, a third-degree polynomial function has
168 been fitted to the data, the respective anomalies are shown in Figure 1 (the original, unfiltered SSN time series is
169 shown in Supplementary Figure 1). The detrended SSN time series has then been correlated (Pearson r) with the
170 detrended tropical stratopause temperature (defined as the mean value between 25°S – 25°N at 1 hPa (Figure 3)). All
171 correlation analyses have been performed by using the Python `scipy.pearsonr` function. Statistical significance of the
172 correlations has been calculated by using a two-tailed Student's t-test, as implemented in Python. In this manuscript
173 we use the term “robust” if a signal of the same sign (e.g., the temperature response at the tropical stratopause)
174 appears in the majority of our ensemble members. To reduce the degree of internal variability, a Butterworth
175 bandpass filter with cutoff frequencies of 9 and 13 years has been applied to the detrended PNJ time series (defined
176 as the arithmetic mean of the zonal-mean zonal wind between 35°N – 45°N at 1 hPa) (Figure 3). The same
177 Butterworth bandpass filter has also been applied to the zonal-mean zonal wind time series at 10 hPa (zonal mean
178 over 55°N – 65°N) (Figure 3) and the NAO time series. The NAO time series has been calculated by the aid of an
179 EOF analysis conducted for the MSLP data over the Atlantic sector (20 – 80°N, 90°W – 40°E) in the winter season
180 (DJF averaged and individually for December, January and February). The first principal component is then used to
181 describe the NAO variability. The lead/lag correlations (Figure 8) are then calculated between the filtered NAO and
182 SSN time series.

183 *Multiple linear regression*

184 To detect the solar cycle signals in the middle atmosphere (Figures 2, 4 and 5) and in the mean sea level pressure in
185 both observations and model data (Figures 6 and 7), we use an established multiple linear regression (MLR) technique
186 as described in Bodeker et al. (1998). To derive the individual regression coefficients, we use a set of six predictors in
187 the MLR model:

188
$$X(t) = \text{Off.const} + A * \text{CO2}(t) + B * \text{QBO}(t) + C * \text{QBOorth}(t) + D * \text{SSN}(t) + E * \text{Nino3.4}(t) + F * \text{tau}(t) + R(t)$$

189 with: Off.const = annual cycle; CO₂(t) = increase in the atmospheric CO₂ concentration; QBO(t) = phase of the QBO,
190 defined by the zonal-mean zonal wind in 30 hPa (5°S – 5°N); QBOorth(t) = the orthogonal of QBO(t); SSN(t) = SSN
191 time series; Nino3.4(t) = Nino3.4 times series; tau(t) = optical thickness at 550 nm and R(t) = model residuum. Based
192 on this MLR analysis, we derived the model response to our chosen set of predictors, e.g., the temperature response
193 per unit of the predictor (i.e., K per 1 SSN). To display the model response during solar maximum, we scaled the
194 coefficients to 180 SSN, which is a good approximation for a mean solar cycle amplitude between 1880 and 1999. To
195 detect potential time lags in the response to the solar cycle at the surface, the solar time series has been shifted in such
196 a way that the model response lags the solar forcing by 1 to 4 years. We like to note, that we use the raw (unfiltered)
197 model output as input for our MLR analysis.

198

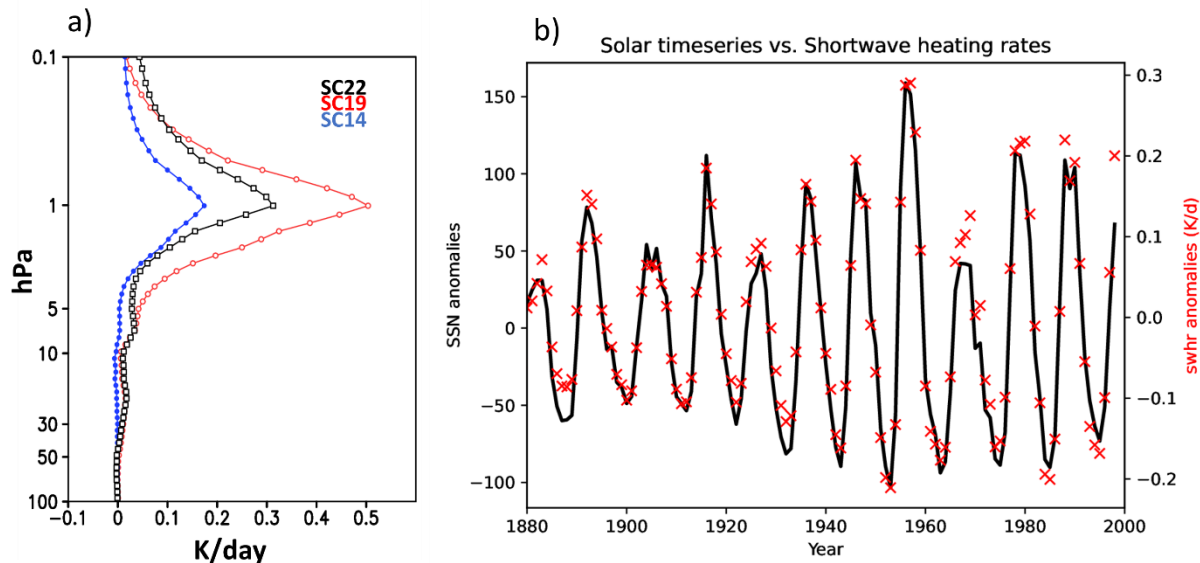
199 **3. The initial radiative solar signal in MPI-ESM**

200 The dynamical “top-down” mechanism, assumed to be the pathway for the propagation of the solar signature through
201 the atmosphere to the surface in NH winter (see also Section 1), is initiated at the tropical upper stratosphere by the
202 absorption of solar ultraviolet (UV) irradiance by ozone and molecular oxygen. In particular, the absorption of solar
203 photons by ozone in the Hartley bands (200 – 310 nm) in the upper stratosphere - and to a lesser extent the Huggins-
204 bands (310 nm – 400 nm) in the middle stratosphere – heats the upper stratosphere increasingly with height and leads
205 to the formation of the warm stratopause. Although the variation in solar UV-irradiance over the 11-year solar cycle
206 is less than 10% in the ozone absorption bands, the enhanced UV radiation at solar maximum – in combination with
207 increased ozone concentrations - leads to stronger shortwave heating and a concurrent warming of the tropical
208 stratopause by the order of 1 K, as has been derived from merged MSU4 and SSU+MLS-satellite observations (Randel
209 et al., 2016).

210 Figure 1a shows the annual mean response of the modelled shortwave radiative heating rate (SWHR) at the
211 stratosphere and lower mesosphere (100 – 0.1 hPa) for a range of solar cycle (SC) amplitudes from the weak SC14 (in
212 blue), over the medium SC22 which has been used as solar forcing in the CMIP5 protocol (in green), to the very strong
213 SC19 (in red). MPI-EMS-HR produces the well-known solar cycle impact with enhanced SW heating during solar
214 maximum throughout the upper stratosphere and lower mesosphere. The maximum SWHR difference develops at the
215 stratopause and ranges for the three selected solar cycles between 0.17 and 0.51 K/day. With a SWHR increase of 0.32

216 K/day for the SC22 solar forcing, MPI-ESM-HR produces an initial solar radiative response at the tropical stratopause
 217 which is in very good agreement with offline radiation model calculations using the CMIP5 solar forcing (i.e., the
 218 same forcing as in MPI-ESM-HR) in a line-by-line reference and two CCM (EMAC and WACCM) radiation codes
 219 (see Figure 8, yellow curves in Matthes et al., 2017). This is a significant improvement compared to the earlier
 220 ECHAM4 and ECHAM5 model versions which were not able to simulate the SWHR response to the solar cycle in the
 221 stratosphere (see Figure 17 in Forster et al., 2011), and thus missed the initial solar temperature signal necessary for
 222 the “top-down” mechanism. The improvement in the MPI-ESM-HR is the result of the enhanced spectral resolution
 223 of the new shortwave radiation scheme in ECHAM6 which resolves the shortwave spectrum in 14 bands spanning the
 224 wavelength range from 820 to 50,000 cm^{-1} (Iacono et al., 2008), whereas ECHAM4 and ECHAM5 used a lower
 225 spectral resolution with the four-band model of Fouquart and Bonnel (1980), later extended to six bands by Cagnazzo
 226 et al. (2007).

227 Figure 1b shows the time series of the SSN and the modeled SWHR at the tropical stratopause over the period from
 228 1880 – 1999. The shown anomalies of both time series from a third-degree polynomial fit clearly demonstrate that
 229 solar cycles of different amplitudes initiate SWHR responses that closely follow in magnitude the strength of the solar
 230 forcing. Only during SC20, the maximum SWHR response is higher than expected for that weak solar cycle. This is
 231 not reproduced in the SWHR, possibly due to the transition from synthetic SSN before 1979 to observed SSN
 232 afterwards.

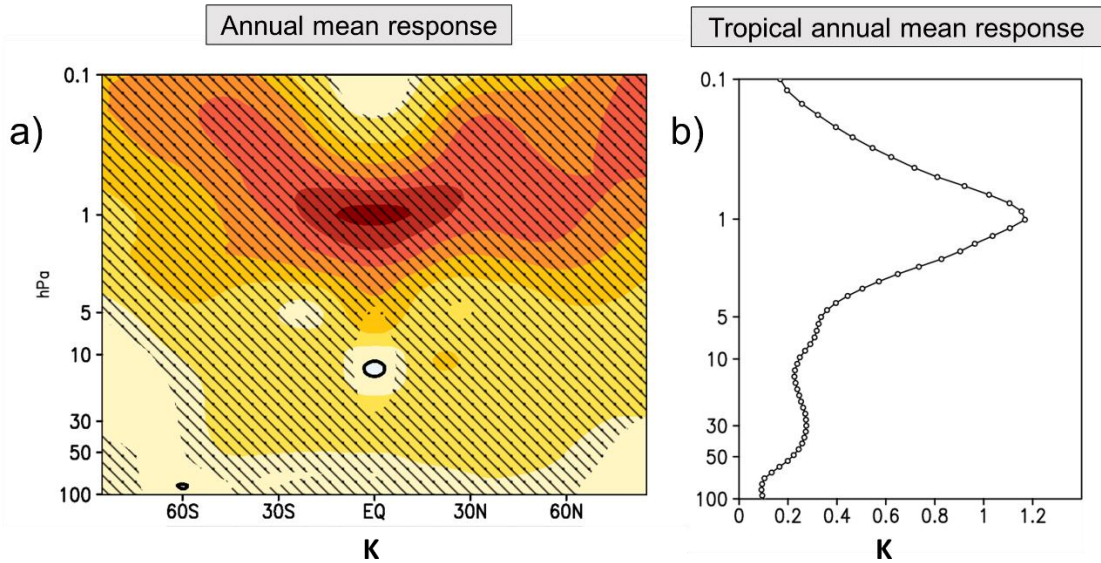


233

234 **Figure 1:** Solar shortwave heating rate signature in the MPI-ESM-HR historical simulations: a) Annual tropical
 235 mean (25°S – 25°N) shortwave heating rate difference in K/day between the maximum and minimum of three solar
 236 cycles: the weak solar cycle 14 (blue), the medium solar cycle 22 used in CMIP5 (green), and the strong solar cycle
 237 19 (red) (a), and: Time series of the sunspot number and the annual tropical mean (25°S – 25°N) shortwave heating
 238 rate at the stratopause (1 hPa). Shown are anomalies from a third-degree polynomial fit to the data (b).
 239

240 When averaging over all solar cycles between 1880 and 1999 and all 10 ensemble members, we obtain a robust, highly
 241 significant annual mean warming of the complete middle atmosphere at solar maximum (Figure 2a), reaching a peak
 242 response of 1.2 K at the tropical stratopause (Figure 2b). This result is slightly higher than the solar signal derived
 243 from satellite observations (0.7 K / 100 solar flux units), respectively ~1 K between solar minimum and maximum)
 244 (Randel et al., 2016). In our simulations we can't find the sometimes observed secondary peak in the temperature in
 245 the lower stratosphere. This secondary peak, however, can no longer be found even in most recent analysis of satellite
 246 data. Dhomse et al. (2022) suggest that the secondary peak (found in earlier studies) emerged most likely due to
 247 aliasing effects related to the Mount Pinatubo eruption in 1991 and probably was not a result of solar variability.
 248 Given the excellent temporal evolution of the initial radiative response of the upper tropical stratosphere to the decadal
 249 solar forcing, we conclude that MPI-ESM-HR produces the necessary prerequisite for the dynamically enhanced “top-
 250 down”-mechanism, which will be investigated in more detail in the next section.

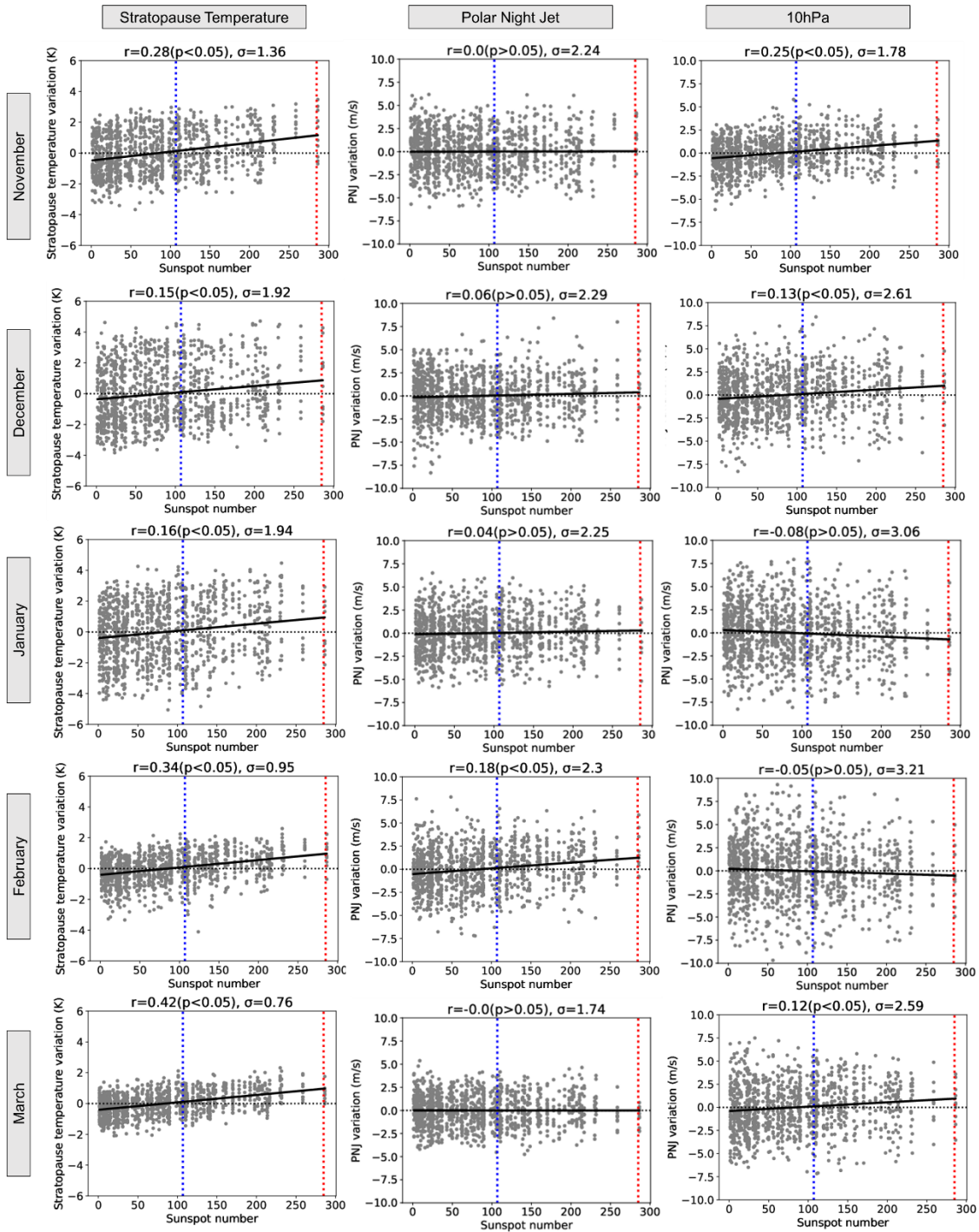
251
 252



253 **Figure 2:** Long-term annual ensemble mean response based on MLR analysis of the zonal-mean temperature (in K)
 254 to the solar cycle in the middle atmosphere as a function of height and latitude (hatched regions mark 95% statistical
 255 significance) (a), and the annual mean tropical (25°S – 25°N) temperature response (in K).
 256
 257

258
259 **4. Downward transfer of the solar signal to the surface: the key role of dynamics**
260
261 After having demonstrated the ability of the MPI-ESM-HR model to realistically simulate the radiative and the related
262 temperature response in the tropical upper stratosphere to the decadal solar forcing, we investigate as next step the
263 potential dynamical reaction to the radiative forcing, which is expected according to the “top-down” mechanism. By
264 evaluating the ensemble spread in the NH during the dynamically active season (November to March), we assess the
265 variability of different dynamical variables in the stratosphere with respect to the solar fluctuations in the MPI-ESM-
266 HR historical ensemble simulations. We focus first on the detrended deviations from the long-term monthly means for
267 the TST and (to estimate the dynamical response in the NH) the zonal-mean zonal wind at two different altitudes and
268 latitudes (Figure 3). To approximate the PNJ (the local maximum wind speed in the upper stratosphere) we use the
269 mean of the zonal-mean zonal wind in 35°– 45°N at 1 hPa. The variability in the middle stratosphere is represented
270 by the mean of the zonal-mean zonal wind in 55°– 65°N at 10 hPa. After calculating the respective anomaly time
271 series for the TST, the PNJ and the 10 hPa zonal wind variations for each month individually, we correlate these time
272 series with the detrended DJF mean SSN time series. To mute the interannual variability (operating on timescales
273 between 1 and 8 years) of the polar vortex, the PNJ and 10 hPa anomaly time series, as well as the SSN time series,
274 have been bandpass-filtered, before calculating the correlations. Please note, that the same SSN time series has been
275 used for the correlation for all individual ensemble members, leading to a “vertical arrangement” of the data in the
276 scatter plots shown in Figure 3. Our results indicate that the TST correlates significantly with the SSN, not only in the
277 annual mean (compare Figure 1b) but also in each individual month considered (Figure 3, left column). While negative
278 and positive TST anomalies (i.e., negative and positive deviations from the long-term monthly mean) are almost
279 uniformly distributed for SSN values smaller than the SC14 maximum (blue dotted lines), an increase in the solar
280 forcing exceeding the SC14 SSN maximum leads to a higher probability of positive TST anomalies. The strength of
281 the correlations changes over the season, such that a stronger connection between the solar forcing and the temperature
282 response at the tropical stratopause is given in late autumn (November: $r=0.28$) and late winter (February: $r=0.34$;
283 March: $r=0.42$). In these months, a particular strong solar forcing (indicated by the SSN value of the SC19 maximum
284 (red dotted lines)) is almost always associated with a positive temperature anomaly at the tropical stratopause. Weaker
285 correlations and a broader distribution of negative and positive temperature anomalies, even during periods with
286 especially pronounced solar activity, are calculated for the midwinter season (December: $r=0.15$; January: $r=0.16$).

287 These findings are consistent with an increase in the overall variability in the TST during December and January,
288 making it more difficult for the relatively weak solar induced signals to be distinguished from the background noise.
289 The higher variability in the TST during December and January is probably a result of the higher variability of the
290 tropical branch of the Brewer-Dobson circulation (BDC) in boreal winter (e.g., Butchart, 2014).
291 According to the general concept of the “top-down” mechanism the initial signal in the TST would be accompanied
292 by a strengthening of the PNJ via a modification of the meridional temperature gradients. Considering the statistically
293 significant temperature signals and correlations at the tropical stratopause in the MPI-ESM-HR model (Figure 3, left
294 column), we expect a dynamical response of the PNJ in our simulations. However, the correlations between the SSN
295 and the PNJ time series (Figure 3, middle column) do not show statistically meaningful relations between the solar
296 forcing and the dynamical response of the PNJ. Only during February, a weak but statistically significant correlation
297 is found, which might be related to the enhanced impact of the solar forcing in the TST during the same month.
298 However, this connection as well becomes insignificant, if the correlations are calculated based on the unfiltered SSN
299 and PNJ time series. Figure 3 (right column) shows the correlations between the solar forcing and the zonal mean
300 zonal wind for the lower (and more northward) 10 hPa anomaly time series. We find the strongest (and significant)
301 correlations in November ($r=0.25$) and December ($r=0.13$), although these correlations become (again) negligible if
302 the correlations are calculated based on unfiltered model data. The differences in the timing between the maximum
303 correlations of the SSN with the PNJ (February) and the 10 hPa zonal wind time series (November and December) are
304 not in line with the established idea of a successive “poleward and downward” progression of the dynamical solar
305 signal. Furthermore, the computed SSN/PNJ correlations for November, December, January and March are ≤ 0.06 ,
306 implying that the characteristics of the PNJ are not markedly influenced by the magnitude of the solar forcing and thus
307 the amplitude of the solar cycle.



308

309 **Figure 3:** Scatter diagram of the stratopause temperature (left column), PNJ (middle column) and zonal-mean zonal
 310 wind averaged over $55^{\circ}\text{N} - 65^{\circ}\text{N}$ at 10 hPa (right column) variations vs. SSN. The numbers given in the headings
 311 show the correlation coefficients (r), their statistical significance ($p < 0.05$: significant correlation, or $p > 0.05$:
 312 insignificant correlation), and the overall variation (σ). The dotted blue and red lines indicate the SSN at solar cycle
 313 maximum for SC14 and SC19 (the weakest/strongest solar cycles considered in the simulations).

314
 315

316 Figure 3 demonstrates that while the connection between the solar forcing and the TST is clearly visible in our
317 correlation analysis, the potential dynamical response in the NH is harder to detect, especially due to the highly variable
318 polar vortex. Therefore, we proceed using a MLR analysis to separate the potential dynamical solar induced signals
319 from other internal generated disturbances in the ensemble mean.

320 After having analyzed the variability of the TST, the PNJ and the 10 hPa zonal-mean zonal wind, we will now isolate
321 potential solar signals by the aid of MLR. Figure 4 shows the solar regression coefficients, scaled to a mean amplitude
322 of the solar cycle (180 SSN), for the zonal-mean temperature (top row), the zonal-mean zonal wind (middle row) and
323 the EPF (vectors) and its divergence EPFD (colors) (bottom row) for each NH winter month (November – March).

324 Here, we focus on the potential solar cycle signals between the equator and the North Pole and pressure heights in
325 1.000 hPa – 0.1 hPa for the temperature and wind responses and 100 hPa – 0.1 hPa for the EPF diagnostics. We find
326 a significant response in the zonal mean temperature at the tropical stratopause (Figure 4, top row) with a maximum
327 response at the equator of 1.2 K during November. The solar induced temperature signal is confined to the inner tropics

328 in late autumn and early winter and advances towards higher latitudes between January and March. This is consistent
329 with the seasonal march of the incidence angle of solar radiation after the winter solstice in December. In the middle
330 to polar latitudes, we find a clear dipole in the temperature anomalies especially during November and December.

331 This dipole is characterized by distinct (and significant) positive temperature anomalies in the lower mesosphere and
332 upper stratosphere and weak (and insignificant) negative anomalies in the middle and lower stratosphere. Particularly
333 the pronounced polar heating in the upper stratosphere from November to December agrees well with a most recent
334 analysis of ERA-interim reanalysis data by Kuroda et al., (2022). The detected temperature signals in the middle

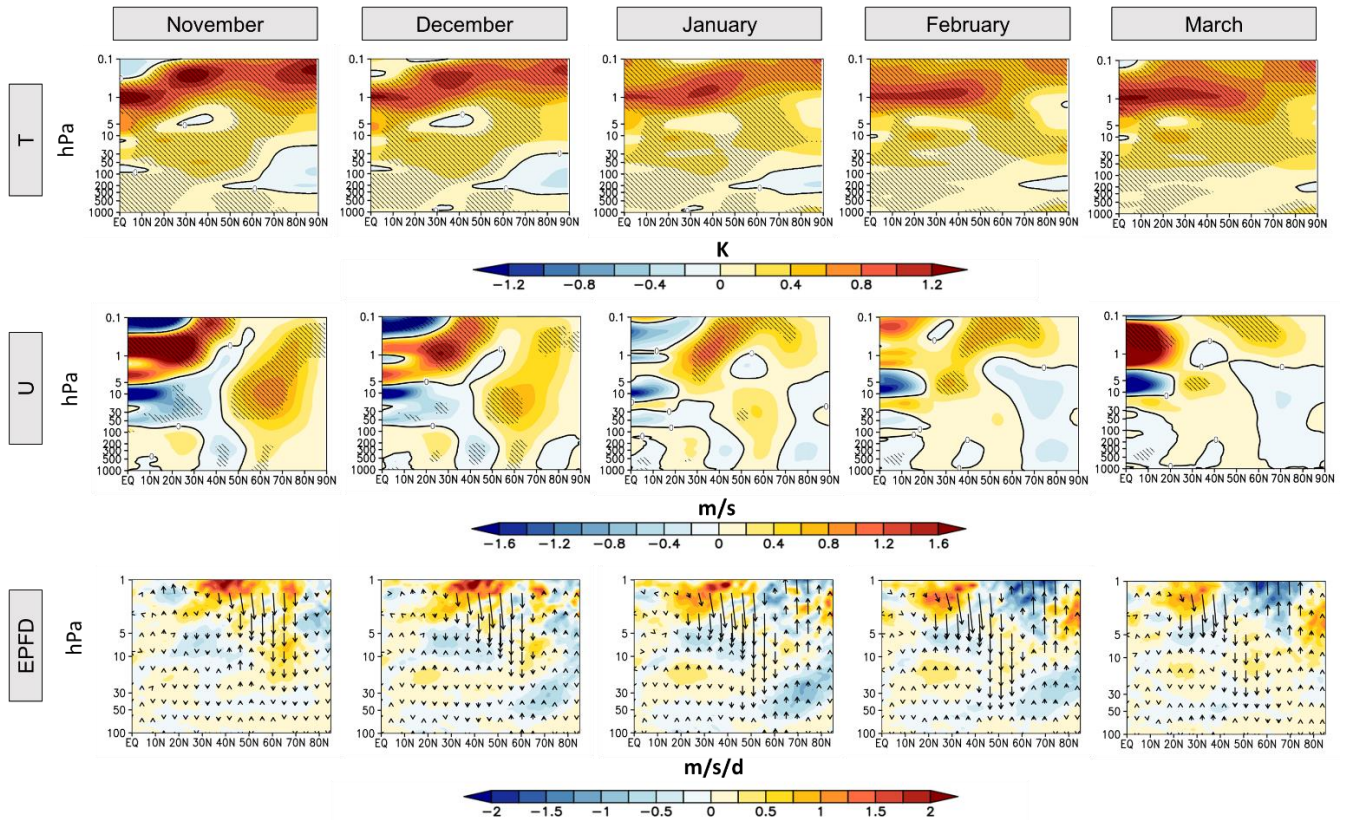
335 atmosphere in November and December are in line with the anomalies in the zonal-mean zonal wind (Figure 4, middle
336 row), which indicate a stronger (and thus cooler) polar vortex during these months. Additionally, a convergence of the
337 EPF (indicated by the reddish colors in Figure 4, bottom row) and its (here downward oriented) vectors imply a reduced
338 upward propagation of planetary waves due to the strengthening of the polar vortex. The maximum (and significant)

339 response in the stratospheric zonal-mean zonal wind in the area of the polar vortex, is located at $\sim 60^\circ\text{N}$ at 10 hPa.
340 Here, we find positive anomalies of the zonal-mean zonal wind of ~ 1 m/s. Given the mean zonal-wind speeds between
341 20 m/s (November) and 30 m/s (December), simulated by the model (not shown) at this height and latitude, the solar
342 influence seems rather small in comparison. The detected dipole in the zonal-mean temperature starts to weaken from

343 January on and vanishes almost completely until March. During the same months, we find a (yet insignificant)

344 weakening of the polar vortex which allows for more upward propagation of planetary waves (indicated by a
345 divergence of the EPF (bluish colors) and upward oriented vectors). In the troposphere, a weak (≤ 0.5 m/s) but
346 significant westerly wind anomaly around $\sim 60^\circ\text{N}$ can be detected in November and December. The weak tropospheric
347 wind response agrees with other studies (Matthes et al., 2006; Schmidt et al., 2010; Ineson et al., 2011; Chiodo et al.,
348 2012; Langematz et al., 2013; Kuroda et al., 2022; Drews et al., 2022).

349 While in some studies the march of the westerly wind anomalies from the middle atmosphere to the surface seems to
350 follow the proposed “poleward and downward” concept (e.g., Matthes et al., 2006; Ineson et al., 2011; Drews et al.,
351 2022), the signal transmission in the MPI-ESM-HR and other model simulations (e.g., Schmidt et al., 2010; Chiodo et
352 al., 2012; Kuroda et al., 2022) rather follows a “downward-only” storyline. Additionally, the description of the
353 westerly wind anomalies at the surface is sometimes inconsistent with the idea of a successive downward propagation
354 of the signal from higher to lower altitudes. As an example, significant westerly wind anomalies at the surface at
355 middle latitudes are already present in November in the modeling studies of Matthes et al. (2006) and Kuroda et al.
356 (2022), even though the major signal is still high up in the middle atmosphere. Furthermore, in Kuroda et al. (2022)
357 the westerly wind anomalies at the surface at middle latitudes are present throughout the complete season (i.e., in all
358 months between November-March), similar to our MPI-ESM-HR simulations. In other studies, the westerly anomalies
359 are insignificant (e.g., Schmidt et al., 2010) or do not reach the ground (e.g., Chiodo et al., 2012). This implies that the
360 detected surface wind anomalies could be independent from the seasonal march in the middle atmosphere and might
361 rather be a product of the internal variability in the troposphere (i.e., the AO or NAO) itself. Likewise, the temperature
362 response to the solar cycle in the troposphere with positive temperature anomalies of ≤ 0.2 K at the surface is rather
363 weak (Figure 4, top row). Interestingly, these small temperature signals are significant in the tropics in all considered
364 months, which is consistent with the high (and relatively constant) solar insolation in the inner tropics and a damped
365 overall variability compared to the extratropical regions. By contrast, the significant surface temperature anomalies in
366 the extratropical regions are located between 50°N and 60°N until January and shift towards the polar latitudes in
367 February and March.



368

369 **Figure 4:** The ensemble mean long-term response (based on MLR) to the solar cycle of the zonal-mean temperature
 370 (first row), zonal-mean zonal wind (second row) (hatched regions mark 95% statistical significance), and the EPF
 371 (vectors) and the divergence of the EPF (EPFD, colors) in the NH during the boreal winter season. All results have
 372 been scaled to 180 SSN.

373

374

375 So far, we focussed on the discussion of the potential solar signals in the ensemble mean derived from the 10 individual
 376 MiKlip historical simulations thus obtaining statistically more robust results than is possible through analyses of single
 377 simulations. The necessity of working with ensemble mean results is impressively demonstrated by comparing two of
 378 our 10 individual ensemble members. Figure 5 shows the solar regression coefficients for the zonal-mean temperature
 379 and zonal-mean zonal wind for the ensemble members 1 (EM1, top panel) and 4 (EM4, bottom panel), as in Figure 4.
 380 The derived patterns for the solar zonal-mean temperature signal in EM1 show distinct similarities with the ensemble
 381 mean. As an example, we find a (significant) maximum temperature response around the tropical stratopause.
 382 Furthermore, the distribution of the temperature anomalies in the middle to higher latitudes again displays the polar
 383 heating in the lower mesosphere and the upper stratosphere and the cooling in the middle to lower stratosphere. Again,
 384 this pattern starts to weaken from January on. We notice that in comparison to the ensemble mean, fewer areas depict

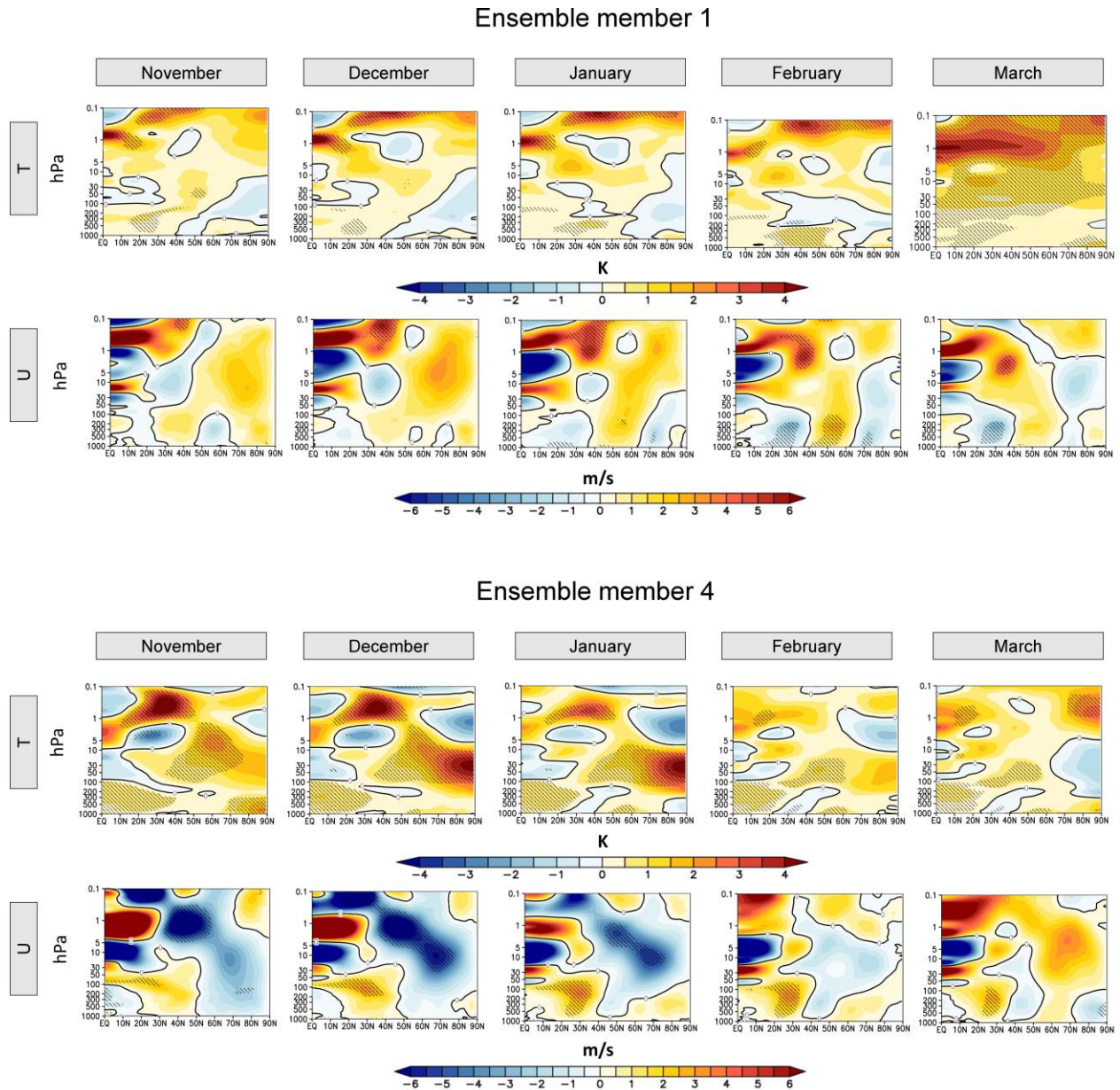
385 significant temperature signals, even though the magnitude of the temperature response is stronger. This can be
386 attributed to the fact that the analysis only includes 120 model years and thus ~12 solar cycles (instead of 1.200 and
387 ~120 in the ensemble mean), which is seemingly not enough to dampen the internal variability and inhibits the solar
388 induced signals to become significant against the overall background noise. Likewise, the solar response of the zonal-
389 mean zonal wind in the middle atmosphere in EM1 shows the main characteristics, as already noticed in the ensemble
390 mean, such as a strengthening of the polar vortex in November and December and a subsequent weakening and a
391 conversion in sign afterwards. However, none of the detected signals in the area of the polar vortex are statistically
392 significant. As for the response of the zonal-mean zonal wind at the surface, we detect significant anomalies in January
393 and February. The geographical distribution of the anomalies (westerly wind anomalies at middle latitudes and easterly
394 wind anomalies at polar latitudes), however, mimic a negative phase of the AO which is not in line with the general
395 concept of solar induced “top-down” influences.

396 In EM4, the initial temperature signal in the upper tropical stratosphere is, as in EM1, visible throughout the complete
397 season and the strongest in November and December. Thus, the response to the solar cycle in these latitudes and
398 heights turns out to be a robust feature in the MPI-ESM-HR model experiments. However, even though exactly the
399 same solar forcing has been applied in EM4 as in EM1, the initial temperature signal is not significant (most likely
400 due to the individual internal variability in this ensemble member) and the dynamical response of EM4 in the
401 extratropical regions looks very different. For instance, we find a cooling of the polar upper stratosphere and a
402 (significant) warming in the middle to lower stratosphere in December and January. This pattern is common during
403 SSWs, which (by chance) could have been more frequent in EM4 during December and January than in EM1. The
404 strong and significant easterly wind anomalies in the middle atmosphere, indicating a slowdown of the polar vortex
405 during these months, underpin this hypothesis. These findings imply that the detected signals in EM1 could also be a
406 result of (by chance) less frequent SSWs in EM1 leading to a potentially misleading attribution to solar variability. In
407 our simulations, four out of 10 simulations show a weakening of the polar vortex during high solar activity, while six
408 depict a strengthening of the latter, which may explain the rather weak tendency to westerly wind anomalies in the
409 ensemble mean.

410 Either way, our results point to the fact that the internal dynamics of the polar vortex have the ability to control the
411 transmission of potential solar induced signals from the tropics to the polar regions and are thus more important than
412 the amplitudes of individual solar cycles (compare also Figure 3), as recently claimed by Drews et al. (2022).

413

414



415

416 **Figure 5:** Long-term response (based on MLR) to the solar cycle of the zonal-mean temperature (first row) and the
417 zonal-mean zonal wind (second row) (hatched regions mark 95% statistical significance) in the two ensemble members
418 EM1 (top panels) and EM4 (bottom panels) in the NH during the boreal winter season. All results have been scaled to
419 180 SSN.

420

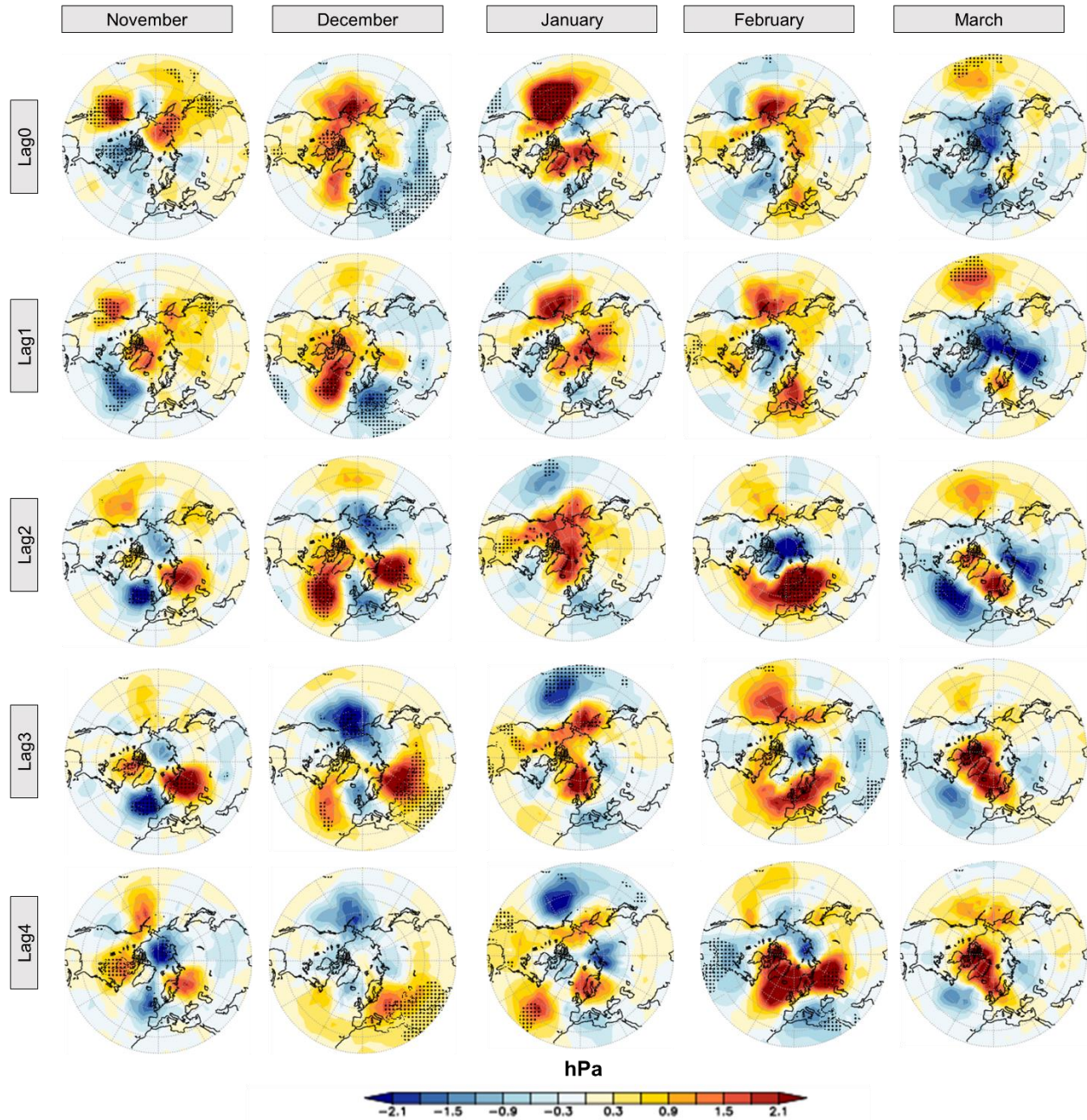
421

422 **5. Direct and lagged surface solar signals**

423 Our results so far indicate a robust response of the TST to the quasi-decadal solar cycle. The subsequent dynamical
424 response in the NH during the boreal winter season, however, is difficult to assess. By the aid of a MLR analysis we
425 could detect weak solar cycle imprints in the zonal-mean temperature and the zonal-mean zonal wind in the ensemble
426 mean. However, these signals are not robust among all individual ensemble members, especially with respect to the
427 detected anomalies in the zonal-mean zonal wind at the surface which seem to be independent of the signals in the
428 middle atmosphere.

429 Nevertheless, in the next step, we first aim at detecting potential solar signals at the surface by applying the MLR
430 analysis to mean sea level pressure (MSLP) data in NH winter. Figure 6 shows the monthly solar regression
431 coefficients for MSLP, scaled to a mean solar cycle amplitude of 180 SSN, in the HadSLP2 observational dataset
432 (Allan and Ansell, 2006) for the same period as simulated (1880 – 1999). In order to check for eventual time lags
433 between the applied solar forcing and the model response, as suggested for example by Gray et al. (2013), lagged
434 regressions were calculated by shifting the solar predictor time series against the observations so that it leads the model
435 data between one and four years. Our results show positive and negative anomalies in the MSLP in the middle and
436 polar latitudes which mimic positive and negative phases of the AO in a rather random than systematic way. As an
437 example, we find an AO-positive like pattern (i.e., negative pressure anomalies over the North Pole and positive
438 pressure anomalies in the surrounding middle latitudes) in November at lag year four, in December at lag year four,
439 in February at the lag years one to three and in March at lag year one. The most pronounced AO-positive anomalies,
440 with a negative but insignificant anomaly of ~ 2 hPa over the North Pole and a positive anomaly of the same magnitude
441 in the middle latitudes, are given at lag year 2. Hence, the strength of the detected potential solar signals in our
442 HadSLP2 analysis is in line with other studies assessing observational products (e.g., Gray et al., 2013; Kuroda et al.,
443 2022; Drews et al., 2022). The detected maximum impact at lag year 2 in February in our analysis, however, agrees
444 with Kuroda et al. (2022) and Drews et al. (2022) but differs from Gray et al. (2013) who found a maximum response
445 at lag year 4 in the DJF mean. These discrepancies in the timing of the peak solar-induced surface signal in the HadSLP
446 MSLP data can only be explained by differences in the analysis techniques, and reveal a high sensitivity of solar-
447 induced surface signals to the applied methodology and individual interpretation of the results. Furthermore, and due
448 to the lack of data covering the whole atmospheric domain over the complete historical period, it is not possible to
449 connect the potential surface solar signals to the seasonality in the middle atmosphere. This applies to our and the
450 original studies (e.g., Gray et al., 2013).

HadSLP2

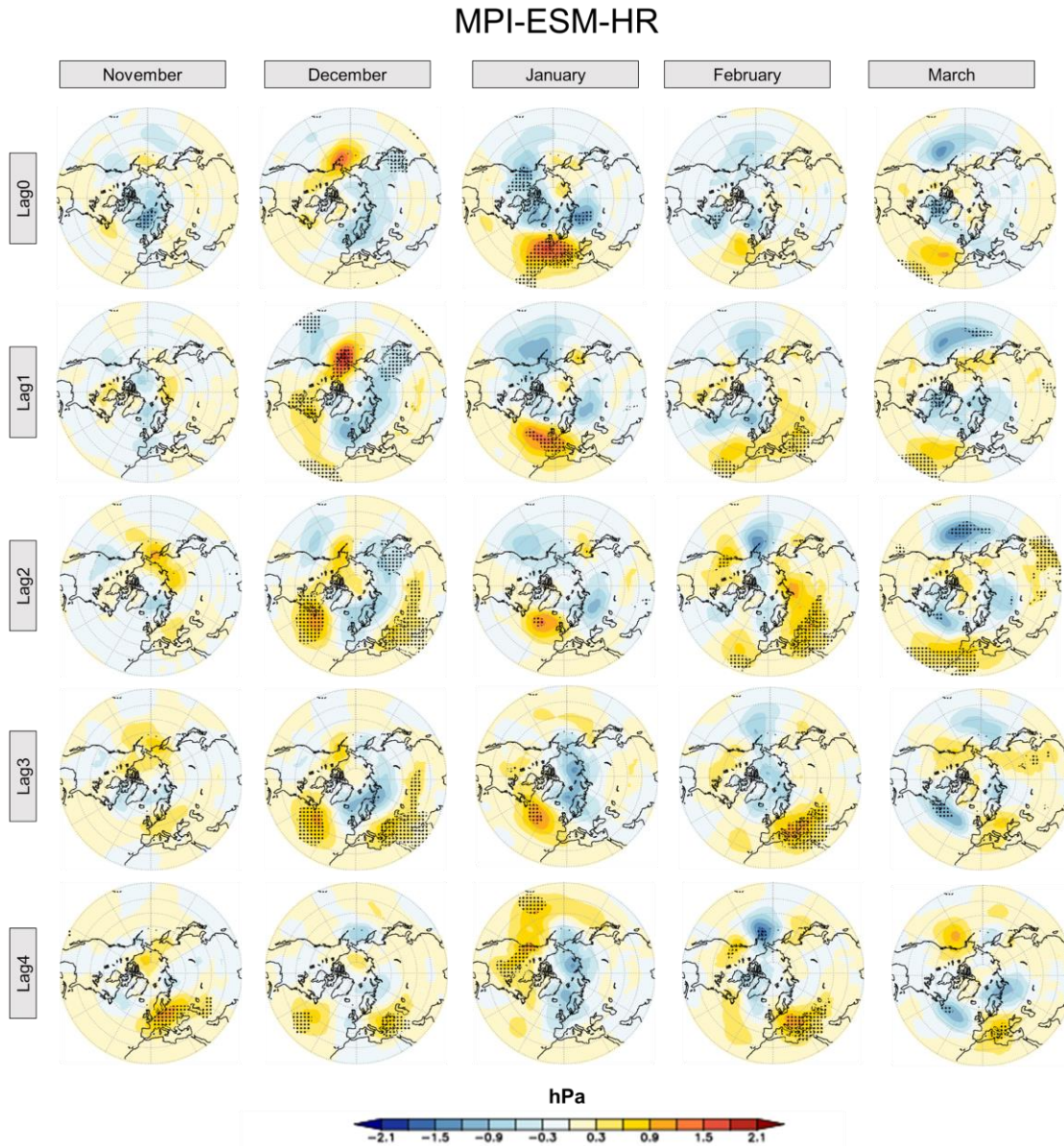


451

452 **Figure 6:** The (lagged) response of mean sea level pressure (MSLP) to the solar cycle in the NH during the boreal
453 winter season for the HadSLP2 dataset (dotted regions mark 95% statistical significance). Columns denote the
454 individual months of the winter season; rows indicate the lag of the MSLP time series with respect to the solar forcing
455 time series.

456

457 Figure 7 shows the same analysis for the MiKlip historical simulations, i.e., the ensemble mean of the solar regression
458 coefficients for the MSLP for each month (November to March) and the (lag) years zero to four. We detect AO-
459 positive-like anomalies in the MSLP in December at the lag years 0 and 1, in January at the lag years 0 to 4 and in
460 February at the lag years zero to four. The strongest negative MSLP anomalies over the North Pole show a response
461 of ~ -1.5 hPa and $\sim +1.5$ hPa in the middle latitudes in January and December. Thus, the overall model response is
462 weaker compared to the observational data. This is not surprising given the fact that the model results depict the mean
463 over 10 ensemble members (with respective dampening effects) compared to one ‘ensemble member’ representing the
464 observations. While the detected magnitudes of the MSLP anomalies in MPI-ESM-HR agree with other solar cycle
465 model studies (e.g. Gray et al., 2013; Scaife et al., 2013; Andrews et al., 2015; Drews et al., 2022), the detected timing
466 (i.e. the progression of the signals from the middle atmosphere to the surface) in the MPI-ESM-HR does not fit the
467 narrative of the “top-down” mechanism as described most recently by Kuroda et al. (2022) and Drews et al. (2022).
468 In these studies, the authors find the most pronounced AO-positive like pattern in February at the surface and link this
469 to the coupling between the stratosphere and the troposphere, which peaks in exactly this month. In contrast, in our
470 model simulations the strongest coupling between the stratosphere and the troposphere appears in December (see
471 Figure 4), while the most pronounced AO-positive like patterns appear in January and February at different lag years.
472 Statistical studies based on MLR analysis of observed and reconstructed MSLP data find both NAO signals in early
473 and late winter at different lags (Grey et al., 2016; Ma et al., 2018). We, therefore, conclude that the detected surface
474 solar signals could rather be a product of the internal variability in the troposphere itself than being necessarily a
475 consequence of the proposed “top-down” mechanism. Even if we assume that the detected surface signals have a pure
476 solar source (and the “top-down” mechanism is always present during solar maximum years) it seems to be
477 questionable in our view if these tiny signals would have the capability to synchronize powerful large-scale climate
478 modes such as the AO or the NAO, if they only emerge once per decade over the duration of a month. As an example,
479 the Icelandic Low and the Azores High, both controlling the pressure gradients in the North Atlantic sector, show a
480 month-by-month variation of ~ 8.5 hPa and ~ 6 hPa during winter time in the model (not shown).



481

482 **Figure 7:** As Figure 6, but for the ensemble mean of the MPI-ESM-HR MiKlip historical simulations.

483

484 **6 A synchronization of the NAO by the solar cycle?**

485 In the following, we will address the question, if the quasi-decadal variations of the solar cycle have the ability to
 486 synchronize the decadal component of the NAO, as proposed by Thiéblemont et al., (2015) and Drews et al., (2022).

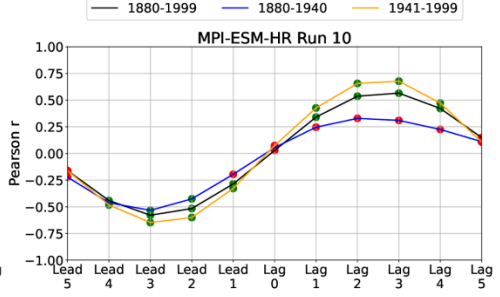
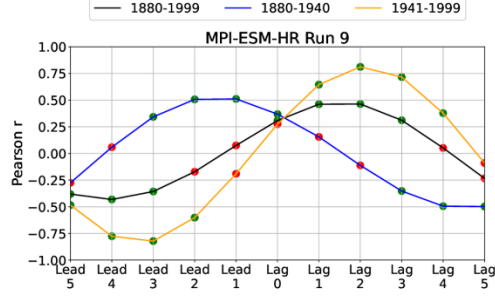
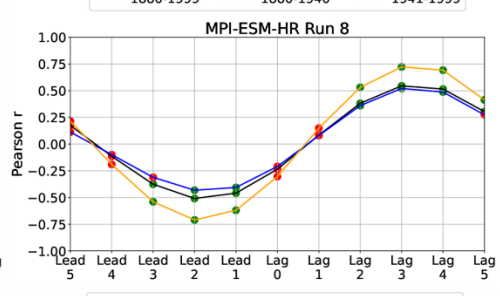
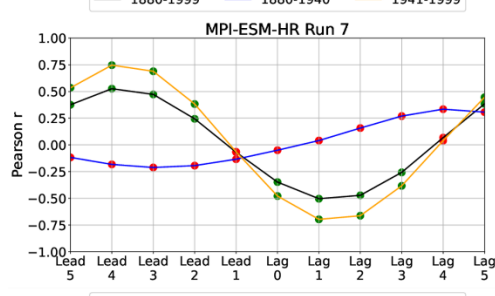
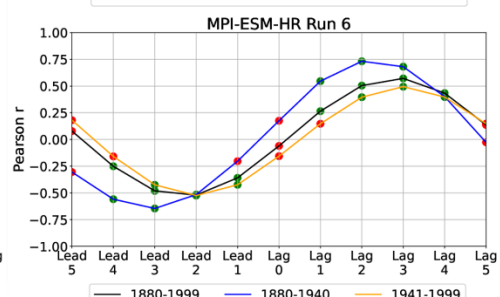
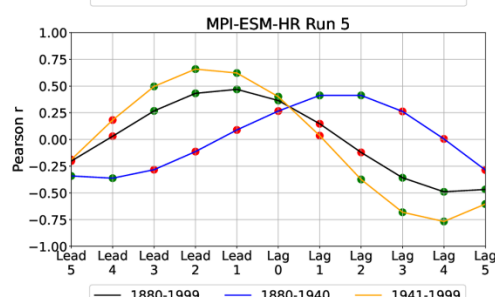
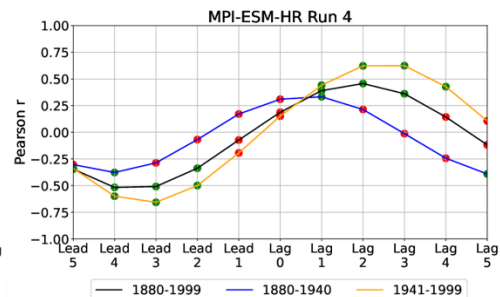
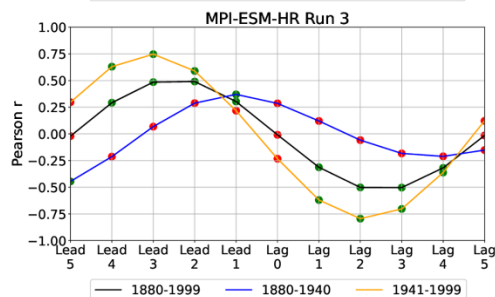
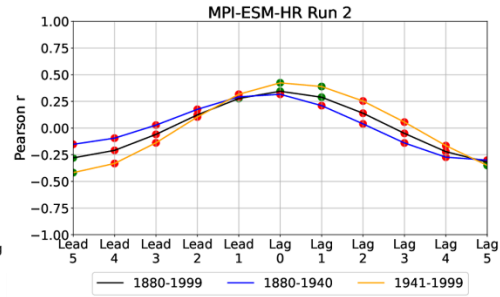
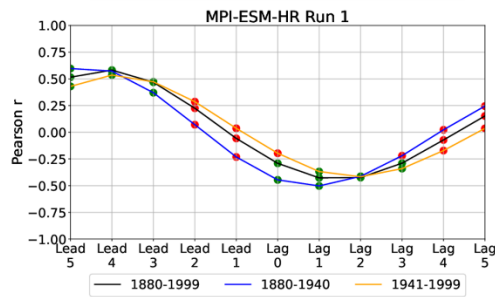
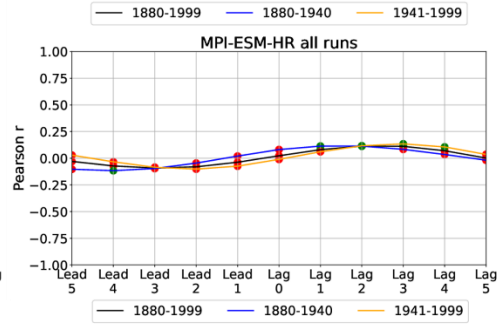
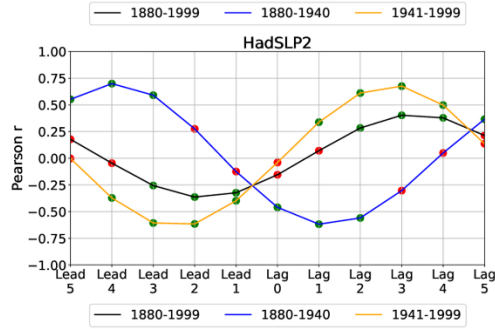
487 For a better comparison, we apply the same analytical strategy as proposed by Thiéblemont et al. (2015) to our model
 488 simulations and the HadSLP2 data, however with the exception that we use the SSN instead of the F10.7 solar flux

489 times series as a solar proxy. Since both the SSN and F10.7 time series show the same oscillations on the interannual
490 and decadal timescale, this is irrelevant for the interpretation of the results. First, an EOF analysis is applied to the
491 deseasonalized MSLP data over the Atlantic sector ($20 - 80^{\circ}\text{N}$, $90^{\circ}\text{W} - 40^{\circ}\text{E}$) in the winter season (DJF averaged).
492 Before continuing, we compared the spatial pattern of the EOF1 between the modelled and observed data and found
493 good agreement with respect to the centers of action and overall characteristics (not shown). The resulting leading
494 principal components (PC1) are then used to describe the variability of the NAO. To mute major parts of the
495 interannual variability, we apply a Butterworth bandpass filter with cutoff frequencies of 9 and 13 years to the PC1
496 and the SSN time series. As a result, the filtered PC1 and SSN time series only include the oscillations operating on
497 the quasi-decadal timescale. Subsequently, lead/lag correlations are calculated between the bandpass-filtered PC1 and
498 SSN timeseries for both the complete dataset and all individual ensemble members (1 to 10). Drews et al. (2022)
499 recently argued that the correlations would become more meaningful during the course of the 20th century due to a
500 series of solar cycles with stronger amplitudes. We, therefore, compute the correlations for three different time
501 segments: the whole period (WP) (1880 – 1999), the early period (EP) with weaker solar amplitudes (1880 – 1940)
502 and the late period (LP) with more pronounced solar amplitudes (1941 – 1999).

503 For the HadSLP2 dataset (Figure 8, left column/first row) positive correlations between the decadal variation of the
504 NAO and the solar forcing is found for the lag years one to four in both the WP and the LP periods, with maximum
505 correlations at lag year three during the LP. For the EP, we find an out-of-phase relation between the solar time series
506 and the NAO on the decadal timescale. The evaluation of this (1 ensemble member) observational dataset implies that
507 the solar forcing actually leads the surface response by a couple of years and that this relation is more pronounced
508 during phases of higher solar activity. Indeed, similar phase relations in the different time segments are given in
509 individual ensemble members of the MiKlip historical simulations (e.g., EM9 (Figure 8, left column/sixth row).
510 However, phase relations like these seem far from being a robust feature if all model runs are considered. As an
511 example, EM5 (Figure 8, left column/third row) indicates positive correlations between the decadal behavior of the
512 SSN and the NAO time series for the lag years one to three during the EP, while this relation reverses (showing
513 negative correlations) during the WP and LP. This is also true for EM3 (left column/third row) and EM7 (left
514 column/fifth row). Other ensemble members (EM2; Figure 8, right column/second row) suggest a maximization of the
515 solar impact at lag year zero and this independently of the considered period. Furthermore, EM6 (Figure 8, right
516 column/fourth row) indicates stronger positive correlations at positive lag years during the EP than during the LP. The

517 most striking discrepancies, however, come from EM1 (Figure 8, left column/second row) and EM4 (Figure 8, right
518 column/third row). While EM1 shows negative correlations between the solar forcing and the NAO at positive lags
519 (in all time segments), this is vice versa in EM4. These surface responses in EM1 and EM4 are, however, opposite to
520 what would be expected from the polar vortex responses in these two ensemble members (a pronounced strengthening
521 of the polar vortex and a downward propagation of westerly wind anomalies to the surface in EM1, and a weakening
522 of the polar vortex and a downward propagation of easterly wind anomalies to the surface in EM4 during winter (see
523 Figure 5)) and opposite to the ‘top-down mechanism’.

524 When applied to the complete dataset of the MiKlip historical simulations, the correlation analysis yields a weak
525 positive (albeit significant) correlation at the lag years two to four, rather independently of the considered time
526 segment. This, however, should rather be interpreted as a slight (and by chance) overhang to positive correlations in
527 the MiKlip dataset (that could change in a larger ensemble) than a robust physical connection between the solar forcing
528 and the NAO. To verify whether the use of the seasonal mean (DJF) might dampen the solar cycle response, as
529 discussed by Drews et al. (2022), we repeated the analysis for the individual winter months (December, January and
530 February, see Supplementary Figure 21) for the model data. We did not detect stronger connections between the decadal
531 solar forcing and the NAO in the calculations based on individual months compared to the seasonal mean. On the
532 contrary, the correlation analysis based on the December months (i.e., the month where we find the “strongest” “top-
533 down” signals in the middle atmosphere) depicts negative correlations at positive lag years. In summary, given all of
534 these inconsistencies we suspect that there is no robust connection between the quasi-decadal solar oscillations and
535 the respective phase of the NAO in the CMIP5 MiKlip historical ensemble simulations.



537
538 **Figure 8:** Lead/lag-correlations between the seasonal mean (DJF) bandpass filtered PC1 based on NAO and SSN
539 time series. For the HadSLP2 dataset and the ensemble mean of the MPI-ESM-HR historical simulations (top row)
540 and the individual MPI-ESM-HR historical runs (rows 2 to 6) for different periods. Green dots mark statistically
541 significant (95%) correlations.
542

543

544 **7. Summary and discussion**

545 Our analysis of the MiKlip historical ensemble simulations, conducted with the state-of-the-art Earth system model
546 MPI-ESM-HR, revealed robust (and statistically significant) solar signals in the TST (see Figures 1 and 2). The
547 dynamical response to the initial solar temperature signal at the tropical stratopause, in the NH middle to polar latitudes
548 during the boreal winter season, however, showed a large spread among our data. This applies to the variability of the
549 PNJ and the 10 hPa zonal-mean zonal wind time series, which both did not show meaningful correlations with the
550 solar forcing (see Figure 3). When removing other than decadal variability components by MLR analysis, we were
551 able to detect (albeit rather weak) solar signals in the NH winter, in both the ensemble mean zonal-mean temperature
552 and zonal-mean zonal wind, that basically agree with the proposed “top-down” influence of solar variability in the
553 middle atmosphere (see Figure 4). However, the MLR analysis based on individual ensemble members revealed
554 signals of opposite direction (i.e., a strengthening (EM1) or weakening (EM4) of the polar vortex during periods of
555 high solar activity) (see Figure 5). Furthermore, we find indications that the detected anomalies in the zonal-mean
556 zonal wind at the surface are most likely independent of the signals in the middle atmosphere. The alleged surface
557 solar signals in MSLP seem to mimic AO-positive (and AO-negative) patterns rather randomly than in a systematic
558 way. This applies to the HadSLP2 data (Figure 6) and to the model data (Figure 7), which both depict most pronounced
559 an AO-positive pattern in January and February at different lag years however in months, where the strong
560 stratospheric influence (in December) is already weak or even reverses sign in the model (compare Figure 4). With
561 respect to the suggested synchronization between the decadal solar forcing and the NAO (e.g., Thiéblemont et al.,
562 2015) we cannot find any meaningful relations in the MiKlip historical simulations. This is supported by the fact that
563 all ensemble members show very individual phase relations (i.e., positive/negative correlations and maximizations
564 during different lag years) between the solar and the NAO time series. Additionally, more robust correlations could
565 not be achieved in different time segments (i.e., periods with stronger or weaker solar forcing). These findings apply
566 to the seasonal winter mean (DJF) as well as to individual winter months (December, January and February). As a

567 consequence, the detected phase relations in the HadSLP2 dataset should be interpreted carefully with respect to
568 potential physical connections between the solar forcing and the NAO, in particular since the observations represent
569 only one single ensemble member.

570 In summary, we draw four major conclusions:

- 571 1. The decadal variations of the TST in the MiKlip historical simulations are a product of the 11-year solar
572 cycle. In the course of this, an increase in the solar intensity leads to enhanced radiative shortwave heating
573 rates and a warming of the TST. These findings are consistent with other modeling studies concerning the
574 imprints of the 11-year solar cycle in the tropical upper stratosphere (Matthes et al., 2004, 2006; Schmidt et
575 al., 2010; Ineson et al., 2011; Chiodo et al., 2012; Langematz et al., 2013). The solar signals in the TST are
576 statistically significant and robust and were detected by our correlation and MLR analyses.
- 577 2. The dynamical response of the NH during winter in the middle atmosphere shows a weak strengthening of
578 the polar vortex during solar maximum in the ensemble mean in the MLR analysis. However, the signals
579 (especially in the zonal-mean zonal wind) are mostly insignificant and of opposite sign in individual ensemble
580 members, and thus not a robust feature. We suppose that the dynamical background state in the middle
581 atmosphere (i.e., the variability of the polar vortex) seems to play an important role for the transfer of the
582 initial radiative solar signal from the upper tropical stratosphere down to the troposphere in NH winter. The
583 important role of middle atmosphere dynamics in modulating potential solar signals is currently investigated
584 as part of the SOLCHECK project and will be published in a subsequent paper (Wenjuan Huo, personal
585 communication).

586 3. The detected anomalies in the zonal-mean zonal wind and MSLP at the surface seem not to be related to the
587 timing of the seasonal march of the signals in the middle atmosphere and are most likely a manifestation of
588 the internal variability in the troposphere itself.

589 4. Concerning the decadal variations of the NAO and the solar forcing, our results suggest that both are
590 independent from each other. We find a range of phase relations between the NAO and the solar forcing
591 throughout our ensemble members, which implies a random statistical relation rather than a physical sound
592 connection.

593
594 It should be noted that we did not explicitly analyze a potential TSI controlled bottom-up effect on the solar surface
595 signal, as bottom-up effects are rather confined to tropical latitudes with a prolonged influence of the TSI throughout
596 the year (e.g., Meehl et al., 2008). Moreover, potential effects related to energetic particle precipitation are not
597 explicitly included in the MiKlip experiments. Since these effects are known to be rather small and even less
598 understood than the 11-year solar cycle surface imprints, we don't think they would alter our results significantly
599 (please see the introduction section).

600 Since the critical study of Chiodo et al. (2019), the “top-down” mechanism and its surface imprints have been further
601 discussed in the scientific community. It is unquestionable that early studies with GCMs and CCMs found evidence
602 of a “top-down” mechanism in the middle atmosphere which in most cases penetrated into the troposphere in NH
603 winter (Matthes et al., 2004, 2006; Schmidt et al., 2010; Ineson et al., 2011; Chiodo et al., 2012; Langematz et al.,
604 2013). These studies all reproduced more or less the basic features of the “top-down” mechanism, thus confirming the
605 physical mechanisms at work suggested by Kodera and Kodera (2002). In contrast, more recent simulations with
606 CCMs and ESMs do not seem to find statistical responses of surface variables to the decadal solar forcing (e.g., Chiodo
607 et al., 2019; this study). Only Drews et al. (2022) showed a near-surface solar imprint for solar cycles with strong
608 amplitudes. The MiKlip simulations are more in line with Chiodo et al. (2019), who argued that the alleged surface
609 solar signals could be an incidental product which is only detectable during phases with stronger solar cycles. Our
610 results even suggest that robust solar surface imprints are basically absent throughout the complete historical period
611 and are thus not sensitive to the amplitude of individual solar cycles. At this point we would like to emphasize that in

612 contrast to previous studies, the MiKlip simulations represent a transient climate system driven by a realistic (observed)
613 solar forcing thus enhancing the confidence in a comparison of our model results to observations.

614 We suggest that the gradual ‘fading away’ of significant solar near-surface signatures in more up-to-date model studies
615 is closely related to progresses made in model development and computer capacities allowing for ensemble
616 simulations. The early simulations were conducted with fixed lower boundary conditions (i.e., prescribed SSTs from
617 observations or control run experiments) (Matthes et al., 2006; Schmidt et al., 2010; Chiodo et al., 2012). Some applied
618 perpetual conditions for the solar forcing (i.e., perpetual solar maximum vs. perpetual solar minimum) and steady-
619 state conditions for the greenhouse gas forcing (Matthes et al., 2006; Schmidt et al., 2010; Ineson et al., 2011). While
620 these models included the necessary physical mechanisms, i.e., UV radiation codes and middle atmosphere dynamics,
621 to capture the solar UV-induced top-down solar signal, the complex nature of physical and chemical processes and the
622 spectrum of internal variability were reduced. Prescribed SSTs, for example, prevent the model from developing the
623 complete spectrum of interannual variability in the troposphere (e.g., induced by the internal variability of the NAO),
624 which might counteract potential surface solar signals. In addition, steady-state background conditions in atmospheric
625 greenhouse gas concentrations and prescribed ozone depleting substances do not take into account transient adjustment
626 processes in the atmospheric dynamics, which again lead to a reduction of the overall internal variability and maybe
627 an overestimation of solar-induced signals. Moreover, due to more limited computer capacities, the results from the
628 early model studies were mostly based on single simulations.

629 In contrast, our results show that in a state-of-the-art climate model system the potential solar near-surface signals are
630 rather weak, not robust and inconsistent with the timing in the middle atmosphere. One potential reason is the
631 additional variability component introduced into the model by the interactively coupled ocean model. Misios and
632 Schmidt (2012) also showed the impact of an interactive ocean on the simulated solar response in the tropical Pacific
633 region. While individual ensemble simulations produce the expected phase correlation between the NAO and the solar
634 cycle, others show the opposite behavior. Thus, we do not find any convincing evidence in our model simulations of
635 the alleged decadal synchronization between the NAO and the solar forcing, as suggested by Thiéblemont et al. (2015).
636 In our view, the decadal near-surface signals detected in the MiKlip historical simulations are a product of the internal
637 variability in the troposphere itself and not a physical consequence of the “top-down” mechanism.

638 We would further like to mention that a strong reduction of the interannual variability in two basically independent
639 time series – be it by bandpass filtering like in our study or in Thiéblemont et al. (2015), or by using wide running

640 mean windows like in Drews et al. (2022) – will always lead to significant alignments of these two time series at some
641 point, if they are shifted towards each other gradually. Thus, the phase relations in our (and other studies) seem to be
642 a statistical artifact and not the consequence of a physical phase coupling. We also would like to question if the oceanic
643 memory is sensitive enough to store the tiny surface solar signals (even if there are some) for the duration of a complete
644 decade. Hence, in our opinion a much more profound solar forcing would be needed to significantly influence the
645 ocean temperature and thus dynamically driven feedbacks. Such forcings, however, typically operate on the centennial
646 timescale which is characterized by phases of Grands Solar Maxima and Minima (e.g., Spiegl and Langematz (2020)).
647 Also, please keep in mind the strong variability of the main pressure systems in the North Atlantic, which might wipe
648 out potential surface solar signals within a couple of months. Furthermore, and in our opinion, a physically sound
649 explanation for the alleged NAO-solar cycle phase coupling is missing so far. Thus, the claim that an inclusion of the
650 11-year solar cycle would lead to a better understanding of the decadal oscillations in the NH troposphere during
651 winter, is not supported by our analyses of the MiKlip historical ensemble simulations. We would finally like to note
652 that the detection of a significant decadal solar impact on the NAO in winter in the MPI-ESM-HR climate model, as
653 in other climate models, might to some degree suffer from the ‘signal-to-noise paradox’, i.e., a low strength of
654 predictable signals vs. a relatively high level of agreement between modelled and observed variability of the

655 atmospheric circulation, which is particularly evident in the climate variability of the Atlantic sector (Scaife and Smith,
656 2018). Future studies with a distinct focus on the decadal prediction skill might help to confirm our results.

657

658 **Data availability**

659 The main numerical results will be made available upon request by the authors.

660 **Author contributions**

661 TS was in charge in conducting the analysis and writing the manuscript. UL initiated the study and contributed to
662 writing the manuscript. HP and JK were involved in conducting the MiKlip historical simulations and writing the
663 manuscript

664 **Competing interests**

665 The authors do not declare any competing interests.

666 **Acknowledgements**

667 We like to thank the DKRZ for granting the computational resources during MiKlip.

668 **Financial support**

669 BMBF funded projects MiKlip-2 (Förderkennzeichen 01LP1517A and 01LP1519A) and SOLCHECK
670 (Förderkennzeichen 01LG1906C)

671 **Review statement**

672 We would like to thank Wenjuan Huo and the anonymous reviewer for taking the time to carefully review our
673 manuscript.

674

675 **References**

- 676 Allan, R., and Ansell, T.: A new globally complete monthly historical gridded mean sea level pressure dataset
677 (HadSLP2): 1850–2004. *J. Climate*, 19(22), 5816-5842, doi.org/10.1175/JCLI3937.1, 2006.
- 678 Andrews, D. G.: Wave–mean-flow interaction in the middle atmosphere. In *Adv. Geophys.* (Vol. 28, pp. 249-275).
679 Elsevier, [doi.org/10.1016/S0065-2687\(08\)60226-5](https://doi.org/10.1016/S0065-2687(08)60226-5), 1985.
- 680 Andrews, M. B., Knight, J. R., and Gray, L. J.: A simulated lagged response of the North Atlantic Oscillation to the
681 solar cycle over the period 1960–2009. *Environ. Res. Lett.*, 10(5), 054022, doi.org/10.1088/1748-9326/10/5/054022,
682 2015.
- 683 Arsenovic, P., Rozanov, E., Stenke, A., Funke, B., Wissing, J. M., Mursula, K., ... and Peter, T.: The influence of
684 Middle Range Energy electrons on atmospheric chemistry and regional climate. *J Atmos Sol Terr Phys.*, 149,
685 180-190, doi.org/10.1016/j.jastp.2016.04.008, 2016.
- 686 Baldwin, M. P., and Dunkerton, T. J.: Stratospheric harbingers of anomalous weather regimes. *Science*, 294(5542),
687 581-584. [doi:10.1126/science.1063315](https://doi.org/10.1126/science.1063315), 2001.
- 688 Baumgaertner, A. J., Jöckel, P., Riede, H., Stiller, G. and Funke, B.: Energetic particle precipitation in
689 ECHAM5/MESy–Part 2: Solar proton events. *Atmos. Chem. Phys.*, 10(15), 7285-7302, [doi.org/10.5194/acp-](https://doi.org/10.5194/acp-10-7285-2010)
690 [10-7285-2010](https://doi.org/10.5194/acp-10-7285-2010), 2010.
- 691 Bodeker, G. E., Boyd, I. S., and Matthews, W. A.: Trends and variability in vertical ozone and temperature profiles
692 measured by ozonesondes at Lauder, New Zealand: 1986–1996. *J. Geophys. Res.*, 103(D22), 28661-28681,
693 doi.org/10.1029/98JD02581, 1998.
- 694 Butchart, N.: The Brewer-Dobson circulation. *Rev. Geophys.*, 52(2), 157-184,
695 <https://doi.org/10.1002/2013RG000448>, 2014.
- 696 Cagnazzo, C., Manzini, E., Giorgetta, M. A., Forster, P. M. D. F., and Morcrette, J. J.: Impact of an improved
697 shortwave radiation scheme in the MAECHAM5 General Circulation Model, *Atmos. Chem. Phys.*, 7, 2503–
698 2515, <https://doi.org/10.5194/acp-7-2503-2007>, 2007.

699 Cionni, I., Eyring, V., Lamarque, J. F., Randel, W. J., Stevenson, D. S., Wu, F., ... and Waugh, D. W.: Ozone
700 database in support of CMIP5 simulations: results and corresponding radiative forcing. *Atmos. Chem. Phys.*,
701 11(21), 11267-11292, doi.org/10.5194/acp-11-11267-2011, 2011.

702 Chiodo, G., Calvo, N., Marsh, D. R., and Garcia-Herrera, R.: The 11 year solar cycle signal in transient simulations
703 from the Whole Atmosphere Community Climate Model. *J. Geophys. Res.*, 117(D6),
704 doi.org/10.1029/2011JD016393, 2012.

705 Chiodo, G., Oehrlein, J., Polvani, L. M., Fyfe, J. C., and Smith, A. K.: Insignificant influence of the 11-year solar
706 cycle on the North Atlantic Oscillation. *Nat. Geosci.*, 12(2), 94-99, doi.org/10.1038/s41561-018-0293-3, 2019.

707 Dhomse, S. S., Chipperfield, M. P., Feng, W., Hossaini, R., Mann, G. W., Santee, M. L. and Weber, M.: A single-
708 peak-structured solar cycle signal in stratospheric ozone based on Microwave Limb Sounder observations and
709 model simulations. *Atmospheric Chemistry and Physics*, 22(2), 903-916, doi.org/10.5194/acp-22-903-2022,
710 2022.

711 Drews, A., Huo, W., Matthes, K., Kodera, K., and Kruschke, T.: The Sun's role in decadal climate predictability in
712 the North Atlantic. *Atmos. Chem. Phys.*, 22(12), 7893-7904, doi.org/10.5194/acp-22-7893-2022, 2022.

713 Eyring, V., Lamarque, J. F., Hess, P., Arfeuille, F., Bowman, K., Chipperfield, M. P., ... and Young, P. Y.: Overview
714 of IGAC/SPARC Chemistry-Climate Model Initiative (CCMI) community simulations in support of upcoming
715 ozone and climate assessments. *SPARC newsletter*, 40 (Januar), 48-66, 2013.

716 Forster, P. M., et al.: Evaluation of radiation scheme performance within chemistry climate models, *J. Geophys.*
717 *Res.*, 116, D10302, [doi:10.1029/2010JD015361](https://doi.org/10.1029/2010JD015361), 2011.

718 Fouquart, Y., and Bonnel, B.: Computations of solar heating of the earth's atmosphere—A new parameterization,
719 *Beitr. Phy. Atmos.*, 53, 35–62, 1980.

720 Gray, L. J., et al.: Solar influences on climate, *Rev. Geophys.*, 48, RG4001, [doi:10.1029/2009RG000282](https://doi.org/10.1029/2009RG000282), 2010.

721 Gray, L. J., Scaife, A. A., Mitchell, D. M., Osprey, S., Ineson, S., Hardiman, S., ... and Kodera, K.: A lagged
722 response to the 11 year solar cycle in observed winter Atlantic/European weather patterns. *J. Geophys. Res.*,
723 118(24), 13-405, doi.org/10.1002/2013JD020062, 2013.

724 Gray, L. J., Woollings, T. J., Andrews, M. and Knight, J.: Eleven-year solar cycle signal in the NAO and
725 Atlantic/European blocking. *Q.J.R. Meteorol. Soc.*, 142: 1890-1903, <https://doi.org/10.1002/qj.2782>, 2016.

726 Huang, J., Hitchcock, P., Maycock, A. C., McKenna, C. M., and Tian, W.: Northern hemisphere cold air outbreaks
727 are more likely to be severe during weak polar vortex conditions. *Communications Earth and Environment*,
728 2(1), 147. doi.org/10.1038/s43247-021-00215-6, 2021.

729 Iacono, M. J., Delamere, J.S., Mlawer, E.J., Shephard, M. W., Clough, S. A., and Collins, W. D.: Radiative forcing
730 by long-lived greenhouse gases: Calculations with the AER radiative transfer models, *J. Geophys. Res.*, 113,
731 D13103, [doi:10.1029/2008JD009944](https://doi.org/10.1029/2008JD009944), 2008.

732 Ilyina, T., Six, K. D., Segschneider, J., Maier-Reimer, E., Li, H., and Núñez-Riboni, I.: Global ocean
733 biogeochemistry model HAMOCC: Model architecture and performance as component of the MPI-Earth system
734 model in different CMIP5 experimental realizations. *J. Adv. Model. Earth Syst.*, 5(2), 287-315,
735 doi.org/10.1029/2012MS000178, 2013.

736 Ineson, S., Scaife, A. A., Knight, J. R., Manners, J. C., Dunstone, N. J., Gray, L. J., and Haigh, J. D.: Solar forcing of
737 winter climate variability in the Northern Hemisphere. *Nat. Geosci.*, 4(11), 753-757, doi.org/10.1038/ngeo1282,
738 2011.

739 Jackman, C. H., Marsh, D. R., Vitt, F. M., Garcia, R. R., Randall, C. E., Fleming, E. L. and Frith, S. M.: Long-term
740 middle atmospheric influence of very large solar proton events. *J. Geophys. Res.*, 114(D11),
741 doi.org/10.1029/2008JD011415, 2009.

742 Jungclaus, J. H., Fischer, N., Haak, H., Lohmann, K., Marotzke, J., Matei, D., ... and Von Storch, J. S.:
743 Characteristics of the ocean simulations in the Max Planck Institute Ocean Model (MPIOM) the ocean
744 component of the MPI-Earth system model. *J. Adv. Model. Earth Syst.*, 5(2), 422-446,
745 doi.org/10.1002/jame.20023, 2013.

746 Kodera, K.: Solar cycle modulation of the North Atlantic Oscillation: Implication in the spatial structure of the
747 NAO. *Geophys. Res. Lett.*, 29(8), 59-1, doi.org/10.1029/2001GL014557, 2002.

748 Kodera, K., and Kuroda, Y.: Dynamical response to the solar cycle. *J. Geophys. Res.*, 107(D24),
749 doi.org/10.1029/2002JD002224, ACL-5. 2002.

750 Kuroda, Y., Kodera, K., Yoshida, K., Yukimoto, S., & Gray, L.: Influence of the solar cycle on the North Atlantic
751 Oscillation. *J. Geophys. Res.*, 127(1), e2021JD035519, doi.org/10.1029/2021JD035519, 2022.

752 Langematz, U., Kubin A., Brühl, C., Baumgaertner, A.J.G., Cubasch, U., and Spangehl, T.: Solar effects on
753 chemistry and climate including ocean interactions, in *Climate And Weather of the Sun-Earth System*
754 (CAWSES): Highlights from a Priority Program, F.-J. Lübken, ed., Springer, Dordrecht, The Netherlands, 2013.

755 Lean, J.: Evolution of the Sun's spectral irradiance since the Maunder Minimum. *Geophys. Res. Lett.*, 27(16), 2425-
756 2428, doi.org/10.1029/2000GL000043, 2000.

757 Ma, H., Chen, H., Gray, L., Zhou, L., Li, X., Wang, R. and Zhu, S.: Changing response of the North
758 Atlantic/European winter climate to the 11-year solar cycle. *Environ. Res. Lett.*, 13(3), 034007,
759 [doi10.1088/1748-9326/aa9e94](https://doi.org/10.1088/1748-9326/aa9e94), 2018.

760 Marotzke, J., Müller, W. A., Vamborg, F. S., Becker, P., Cubasch, U., Feldmann, H., ... and Ziese, M.: MiKlip: a
761 national research project on decadal climate prediction. *Bull. Am. Meteorol. Soc.*, 97(12), 2379-2394,
762 <https://doi.org/10.1175/BAMS-D-15-00184.1>, 2016.

763 Matthes, K., Langematz, U., Gray, L. L., Kodera, K., and Labitzke, K.: Improved 11-year solar signal in the Freie
764 Universität Berlin climate middle atmosphere model (FUB-CMAM). *J. Geophys. Res.*, 109(D6),
765 doi.org/10.1029/2003JD004012, 2004.

766 Matthes, K., Kuroda, Y., Kodera, K., and Langematz, U.: Transfer of the solar signal from the stratosphere to the
767 troposphere: Northern winter. *J. Geophys. Res.*, 111(D6), doi.org/10.1029/2005JD006283, 2006.

768 Matthes, K., Funke, B., Andersson, M. E., Barnard, L., Beer, J., Charbonneau, P., Clilverd, M. A., Dudok de Wit, T.,
769 Haberreiter, M., Hendry, A., Jackman, C. H., Kretzschmar, M., Kruschke, T., Kunze, M., Langematz, U.,
770 Marsh, D. R., Maycock, A. C., Misios, S., Rodger, C. J., Scaife, A. A., Seppälä, A., Shangguan, M., Sinnhuber,
771 M., Tourpali, K., Usoskin, I., van de Kamp, M., Verronen, P. T., and Versick, S.: Solar forcing for CMIP6
772 (v3.2), *Geosci. Model Dev.*, 10, 2247–2302, doi.org/10.5194/gmd-10-2247-2017, 2017.

773 Meehl, G. A., J. M. Arblaster, G. Branstator, and H. van Loon: A Coupled Air–Sea Response Mechanism to Solar
774 Forcing in the Pacific Region. *J. Climate*, 21, 2883–2897, <https://doi.org/10.1175/2007JCLI1776.1>, 2008.

775 Meehl, G. A., Goddard, L., Boer, G., Burgman, R., Branstator, G., Cassou, C., ... and Yeager, S.; Decadal climate
776 prediction: an update from the trenches. *Bull. Am. Meteorol. Soc.*, 95(2), 243-267, [doi.org/10.1175/BAMS-D-](https://doi.org/10.1175/BAMS-D-12-00241.1)
777 [12-00241.1](https://doi.org/10.1175/BAMS-D-12-00241.1), 2014.

778 Mehta, V., Meehl, G., Goddard, L., Knight, J., Kumar, A., Latif, M., ... and Stammer, D.: Decadal climate
779 predictability and prediction: where are we?. *Bull. Am. Meteorol. Soc.*, 92(5), 637-640,
780 doi.org/10.1175/2010BAMS3025.1, 2011.

781 Misios, S. and Schmidt, H.: Mechanisms Involved in the Amplification of the 11-yr solar cycle signal in the tropical
782 Pacific Ocean, *J. Climate*, 25, 5102–5118, doi.org/10.1175/JCLID-11-00261.1, 2012.

783 Müller, W. A., Jungclaus, J. H., Mauritsen, T., Baehr, J., Bittner, M., Budich, R., ... and Marotzke, J.: A higher-
784 resolution version of the max planck institute earth system model (MPI-ESM1. 2-HR). *J. Adv. Model. Earth*
785 *Syst.*, 10(7), 1383-1413, doi.org/10.1029/2017MS001217, 2018.

786 Paulsen, H., Ilyina, T., Six, K. D., and Stemmler, I.: Incorporating a prognostic representation of marine nitrogen
787 fixers into the global ocean biogeochemical model HAMOCC. *J. Adv. Model. Earth Syst.*, 9(1), 438-464,
788 doi.org/10.1002/2016MS000737, 2017.

789 Pohlmann, H., Müller, W. A., Kulkarni, K., Kameswarrao, M., Matei, D., Vamborg, F. S. E., Kadow, C., Illing, S.,
790 and Marotzke, J.: Improved forecast skill in the tropics in the new MiKlip decadal climate predictions, *Geophys.*
791 *Res. Lett.*, 40, 5798– 5802, [doi.10.1002/2013GL058051](https://doi.org/10.1002/2013GL058051), 2013.

792 Pohlmann, H., Müller, W. A., Bittner, M., Hettrich, S., Modali, K., Pankatz, K., and Marotzke, J.: Realistic quasi-
793 biennial oscillation variability in historical and decadal hindcast simulations using CMIP6 forcing. *Geophys.*
794 *Res. Lett.*, 46(23), 14118-14125, doi.org/10.1029/2019GL084878, 2019.

795 Randel, W. J., Smith, A. K., Wu, F., Zou, C., and Qian, H.: Stratospheric Temperature Trends over 1979–2015
796 Derived from Combined SSU, MLS, and SABER Satellite Observations, *J. Climate*, 29(13), 4843-4859,
797 doi.org/10.1175/JCLI-D-15-0629.1, 2016.

798 Reick, C. H., Raddatz, T., Brovkin, V., and Gayler, V.: Representation of natural and anthropogenic land cover
799 change in MPI-ESM. *J. Adv. Model. Earth Syst.*, 5(3), 459-482, doi.org/10.1002/jame.20022, 2013.

800 Scaife, A. A., Ineson, S., Knight, J. R., Gray, L., Kodera, K., and Smith, D. M.: A mechanism for lagged North
801 Atlantic climate response to solar variability. *Geophys. Res. Lett.*, 40(2), 434-439, doi.org/10.1002/grl.50099,
802 2013.

803 Scaife, A. A. and Smith, D.: A signal-to-noise paradox in climate science. *NPJ Climate and Atmospheric Science*,
804 1(1), 28, [doi:10.1038/s41612-018-0038-4](https://doi.org/10.1038/s41612-018-0038-4), 2018.

805 Seppälä, A., Randall, C. E., Clilverd, M. A., Rozanov, E., & Rodger, C. J.: Geomagnetic activity and polar surface
806 air temperature variability. *J. Geophys. Res.*, 114(A10), doi.org/10.1029/2008JA014029, 2009.

807 Seppälä, A., Matthes, K., Randall, C. E. and Mironova, I. A.: What is the solar influence on climate? Overview of
808 activities during CAWSES-II. *Progress in Earth and Planetary Science*, 1(1), 1-12, [doi.org/10.1186/s40645-014-](https://doi.org/10.1186/s40645-014-0024-3)
809 [0024-3](https://doi.org/10.1186/s40645-014-0024-3), 2014.

810 Schmidt, H., Brasseur, G. P., and Giorgetta, M. A.: Solar cycle signal in a general circulation and chemistry model
811 with internally generated quasi-biennial oscillation. *J. Geophys. Res.*, 115(D1), doi.org/10.1029/2009JD012542,
812 2010.

813 Spiegl, T. and Langematz, U.: Twenty-First-Century Climate Change Hot Spots in the Light of a Weakening Sun.
814 *Journal of Climate*, 33(9), 3431-3447, doi.org/10.1175/JCLI-D-19-0059.1, 2020.

815 Stevens, B., et al.: Atmospheric component of the MPI-M Earth System Model: ECHAM6, *J. Adv. Model. Earth*
816 *Syst.*, 5, 146–172, [doi:10.1002/jame.20015](https://doi.org/10.1002/jame.20015), 2013.

817 Taylor, K. E., Stouffer, R. J., and Meehl, G. A.: An overview of CMIP5 and the experiment design. *Bull. Am.*
818 *Meteorol. Soc.*, 93(4), 485-498. doi.org/10.1175/BAMS-D-11-00094.1, 2012.

819 Thiéblemont, R., Matthes, K., Omrani, N. E., Kodera, K., and Hansen, F.: Solar forcing synchronizes decadal North
820 Atlantic climate variability. *Nat. Commun.*, 6(1), 8268, [doi:10.1038/ncomms9268](https://doi.org/10.1038/ncomms9268), 2015.

821

822